Blood Microflow Characterization

Using Micro-Particle Image Velocimetry and 2-Beam Fluorescence Cross-Correlation Spectroscopy

Andy Vinh Le

Thesis submitted to the University of Ottawa
in partial fulfillment of the requirements for the
M.A.Sc. in Mechanical Engineering

The Ottawa-Carleton Institute for Mechanical and Aerospace Engineering
Faculty of Engineering
University of Ottawa

Acknowledgements

I would like to thank everyone who contributed in helping me make this project possible and a success.

First, I would like to thank my supervisor, Dr. Marianne Fenech, for her guidance and support throughout my project. Her advice and expertise have helped me overcome many obstacles throughout my research journey. Without her, I would not have had the wonderful experiences and the opportunity to complete another international experience.

I also would like to thank Dr. Manouk Abkarian from the Centre de Biologie Structurale in Montpellier for hosting me in his lab for the international internship and allowing me to use their FCS setup. His expertise and guidance were invaluable in developing a better understanding of blood rheology. I am also thankful to Dr. Emmanuel Margeat from the Centre de Biologie Structurale for providing his expertise and guidance on FCS.

I am very grateful to all the people that I have met through the Fenech's Laboratory group, the conversation on various research and work has been enlightening. A special thanks to Curtis James Karns Armstrong for his PDMS epoxy molds used for the μPIV experiment and his insight on the experimental procedure of the measurement techniques.

I would especially like to express my gratitude to my friends and family for their continued support throughout my journey. They kept me going on and this work would not be possible without their words of encouragement.

Statement of Ethics

The research conducted involving human subjects was done with the approval of the ethics committee of the University of Ottawa (H-03-19-3441).

Abstract

Abstract - Blood flow through microcirculation in both simple and complex geometry has been difficult to predict due to the composition and complex behavior of blood at the microscale. Blood is a dense suspension of deformable red blood cells that is comparable in dimensions to the microchannels that it flows through. As a result, rheological properties at the microscale can vastly differ from bulk rheological properties due to non-continuum effects. To further develop our understanding of blood microflow; experimental techniques should be explored.

In this work, we explore micro-particle image velocimetry (μPIV) and two-beam fluorescence cross-correlation spectroscopy (2bFCCS) in the application of characterizing blood in microflow conditions. For the development of the μPIV analysis, a polydimethylsiloxane co-flow channel is used to observe blood flow in controlled conditions. Flow conditions (velocity profile and blood layer thickness) are selected based on an analytical model and compared to experimental measurement. The experimental results presented indicate that current flow conditions are inadequate in providing a controlled rate of shear on the blood layer in the co-flow channel and further optimization are required to improve the measurement of the velocity profile. For the development of the 2bFCCS application for blood flow analysis, a wide glass capillary microfluidic device is used to complete the verification of fluorescence fluid admissibility, the effect of laser intensity on inducing photobleaching and the velocity measurement performance. The experimental measurement of the velocity profile is validated against the theoretical profile for a rectangular channel. Results of the velocity profile of high concentration red blood cells show promise in the technique's ability to measure blood microflows closer to physiological conditions.

Keywords: microcirculation, hemodynamic, red blood cell, velocity profile, cell free layer, microfluidic device

Table of Contents

List of Tables

List of Figures

List of Symbols

cP	Centipoise
D [μm]	Half-width of channel
dt [μs]	Time interval between laser pulse
d_p [μm]	Tracer particle size
dp/dx [mPa]	Pressure drop
F_1, F_2 [counts per second]	Fluorescence intensity signal in focal volume
$\overline{F_1}, \overline{F_2}$ [counts per second]	Average fluorescence intensity signal in focal volume
$f^{\#}$	Focal number
$G_C(\tau)$	Cross-correlation function
h [μm]	Height of channel
$\bar{I}_A, \bar{I}_B$	PIV averaged images
N	Average molecule number in detection volume
M	Magnification
Q [μl/hr]	Input flow rate
Q_{PBS} [μl/hr]	Flow rate of PBS and glycerol solution
Q_B [μl/hr]	Flow rate of blood sample
R [μm]	Distance between center of two focal volume
$\vec{r}, \overrightarrow{r'}$ [μm]	Spatial coordinates for the two focal volume
$\bar{R}_{AB}$	PIV averaged correlation function
$R_{\overline{AB}}$	PIV image averaging
R_n	PIV correlation functions
t [s]	Time
$u(x)$ [μm/s]	Velocity in the flow direction
V_1, V_2 [μm^3]	Focal volume element
w [μm]	Width of channel
w_0 [μm]	Radius of focal volume
x, y, z [μm]	Incremental distance between fluid layer
Z_{corr} [μm]	Depth of correlation

α [Degrees]	Angle between direction of flow and focal volume
$\dot{\gamma}$ [s^{-1}]	Rate of shear strain
δ [µm]	Location of fluid interface
ϵ	Relative distribution of particle displaced a distance from focal plane
λ [nm]	Wavelength of emitted light
τ [s]	Lag time
τ_F [s]	Flow time defined as ratio between two focal volume and flow velocity
μ, μ_A, μ_B [cP]	Viscosity of specific fluid

List of Abbreviations

APD	Avalanche photodiode
CC	Cell-cell interaction
CCD	Charged coupled device
CFL	Cell-free layer
CW	Cell-wall interaction
EDTA	Ethylenediaminetetraacetic acid
FCS	Fluorescence correlation spectroscopy
HEPES	4-(2-hydroxyethyl)-1-piperazineethanesulfonic acid
HT	Hematocrit
KOH	Potassium hydroxide
PBS	Phosphate buffered saline
PDMS	Polydimethylsiloxane
PIV	Particle image velocimetry
PLL-PEG	Poly(L-Lysine)-PEG methyl ether
RBC	Red blood cells
WBC	White blood cells
µPIV	Micro-particle image velocimetry
2bFCCS	2-beam fluorescence cross-correlation spectroscopy

1 Introduction

1.1 Research Motivation

Blood is an essential type of connective tissue with functions that include transportation of dissolved gases, protection from invading microorganisms and regulation of many bodily processes [1]. Due to the importance of blood, developing an understanding of blood flow phenomena is of great scientific interest especially for the design of biomedical applications such as microfluidic devices and in the understanding of microvascular disorders such as sickle cell disease. However, because of the composition and complex behaviour of blood, much more is still to be discovered about blood flow properties in the microcirculation [1].

Blood is a dense suspension of formed elements suspended in a macromolecule rich aqueous phase known as plasma. The formed elements consist of deformable red blood cells (RBC), white blood cells (WBC), and platelets, in which RBC normally constitutes approximately 40-45% of the total volume [1]. Under low shear conditions, the cells undergo a reversible aggregation between cells which is induced by the presence of macromolecules in the plasma phase. Furthermore, in microcirculation RBC tend to migrate away from walls and towards the center of the channel resulting in a two-phase flow: an inner RBC dense core and a cell free layer at the vessel wall. These two phenomena contribute to the heterogeneous distribution of the RBC in the plasma phase, resulting in interesting rheological properties at both the microscopic and macroscopic scales. Previous research in the field of blood rheology has either been descriptive when observing blood in microcirculation, such as revealing how local RBC volume fraction is heterogenous when split in a microchannel bifurcation [2], or classical, such as when showing blood apparent viscosity decreasing with an increase force on the flow [1, 3].

From classical studies, an understanding of rheological properties of blood such as its non-Newtonian shear thinning characteristics has been known through rheological measurements using rotational viscometers

and small glass capillaries [3]–[5]. However, these studies in simple geometries are still insufficient at predicting blood structures in more complex bulk flow and microcirculatory conditions. The assumptions made for standard rheological measurements to obtain intrinsic properties of the blood do not represent complex fluids well since torque measurement in the rheometer considers the velocity profile to be linear in the measurement. However, for blood, the velocity profile is non-linear due to the heterogeneity of the RBC distribution.

Currently, there lacks a constitutive law that connects the microscopic structure of blood flow with the bulk macroscopic rheological measurements of blood. To further our understanding of the complex nature of blood in both the macroscopic and microscopic scale, new approaches need to be explored. In this thesis, the method of micro-particle image velocimetry and two-beam fluorescence cross-correlation spectroscopy is explored for the application of completing blood rheology measurements.

1.2 Literature Review

This section covers the background information on the characteristics of blood and hemorheology at the microscale, the theoretical formulation of velocity profile in channel geometries used in the study, and an overview of the velocity measurement techniques.

1.2.1 Blood Composition

Whole blood is composed of formed elements suspended in a liquid intercellular matrix. The formed elements consist of RBC, WBC, and platelets. While the suspending liquid known as plasma has dissolved proteins, electrolytes, minerals, and fats. Typically, RBC constitutes approximately 40-45% the total volume of whole blood [1, 6] . RBC contains hemoglobin which is a protein that helps carry oxygen from the lungs to the rest of the body and carbon dioxide from the body to the lungs. WBC which consists of monocytes, lymphocytes, neutrophils, eosinophils and basophils are involved with protecting the body from foreign invaders and infectious diseases [6]. Platelets are fragments of cytoplasm derived from megakaryocytes in bone marrow. They are activated when it is exposed to either high shear stress, or rapid

increases in shear stress which results in the initiation of the coagulation cascade that forms blood clots at sites of injured blood vessels [6]. Lastly, the plasma transports everything from blood cells, nutrients, waste products, hormones, and proteins throughout the body.

1.2.1.1 Red Blood Cells

RBC are specialized cells whose main function is the transportation of oxygen. When formed, the nucleus of the erythroblast is shed before the RBC enters the bloodstream. The typical shape of a normal human RBC is a biconcave disk with an approximate diameter of 8 μm and thickness of about 1 μm to 2 μm from the thinnest region at the center to the thickest region. The biconcave nature of the RBC results in a high surface area to volume ratio and deformable properties. The lack of a nucleus allows RBC to contain more hemoglobin and in combination with the shape allows the cell to maximize its oxygen carrying capacity [1]. While the deformable nature of RBC also allows it to pass through vessels that are narrower than the cells undeformed size[7].

RBC membrane can be considered as a thin, highly deformable viscoelastic shell that consists of an outer lipid bilayer and a mesh like protein cytoskeleton lining the inner surface of the bilayer. The bilayer consists of a hydrophilic head and a hydrophobic tail region. The bilayer strongly resists any area changes that would result in the exposure of the lipids' tail to the aqueous environment. The result is a membrane that behaves like an incompressible material in two dimensions [1]. Due to the fluid nature of the lipid bilayer, the cytoskeleton can move relative to the bilayer when part of the membrane is stretched [1, 8]. The RBC membrane has a thickness less than 10 nm [1, 9].

1.2.1.2 Plasma

Plasma is a dilute electrolyte solution that suspends the formed elements in whole blood. Plasma contains fibrinogen, globulin, and albumin proteins at approximately 8% by weight in water. Fibrinogen is a key protein in the formation of blood clot as it polymerizes into fibrin. Globulin is a protein that is a carrier of lipids and other water-soluble substances and it also contains antibodies that are used to resist infection

from bacteria and viruses. Lastly, albumin is a type of protein that is important in the balance of water metabolism as it is the main contributor to the total osmotic pressure of the plasma proteins. The higher osmotic pressure due to the presence of the protein in the plasma results in the absorption of water from the interstitial fluids into the capillaries. Besides the presence of plasma proteins, plasma is identical to the interstitial fluid in composition [6].

1.2.1.3 Hematocrit

When blood is separated in a centrifuge, the formed elements and suspending fluid are separated due to the density of the components. Starting from the bottom of the tube are the RBC, the densest element, followed by the buffy layer composed of WBC and platelets, and lastly the plasma layer. Hematocrit (HT) is defined as the volume fraction of the blood that is occupied by the RBC. Typical levels of HT ranges from 40-45% [1, 6, 10]. The density of whole blood is approximated to be 1060 kg/m^3.

1.2.2 Hemorheology

The field of hemorheology is the study of deformation and flow of blood and its formed elements. The field investigates blood in both the macroscopic scale where bulk properties of blood are observed and at the microscopic scale where interactions among cellular components occur. The rheological properties of blood are dependent on many factors from the shear rate, to the dimensions and geometry of the vessel that the blood flows through [4]. An understanding of rheological properties of blood such as its non-Newtonian characteristics have been known through rheological studies using rotational viscometers and small glass capillaries [3]–[5]. However, studies in simple geometries are still insufficient at predicting rheological properties in networks such as microcirculation due to the variation of vessel length, diameter, and flow rate. Furthermore, other phenomena of human blood are the formation of RBC aggregates and the formation of a cell-free layer (CFL) in microcirculation.

1.2.2.1 Viscosity

Viscosity is an intrinsic property of a fluid that is related to the rate of deformation that a fluid experiences when a shear stress is applied to it. A common thought experiment is imagining two infinite parallel flat plates separated with a finite height and a fluid in between; a schematic is represented in Figure 1-1. The top plate is movable with an applied force causing it to move at a constant velocity tangentially to the other plate and results in an applied shear stress on the fluid that will continuously deform it under the application of the shearing stress. The velocity gradient of the fluid between the two plates is referred to as the rate of shear strain, and is simply the ratio of incremental velocity change and distance change perpendicular to the direction of shear stress [6, 10].

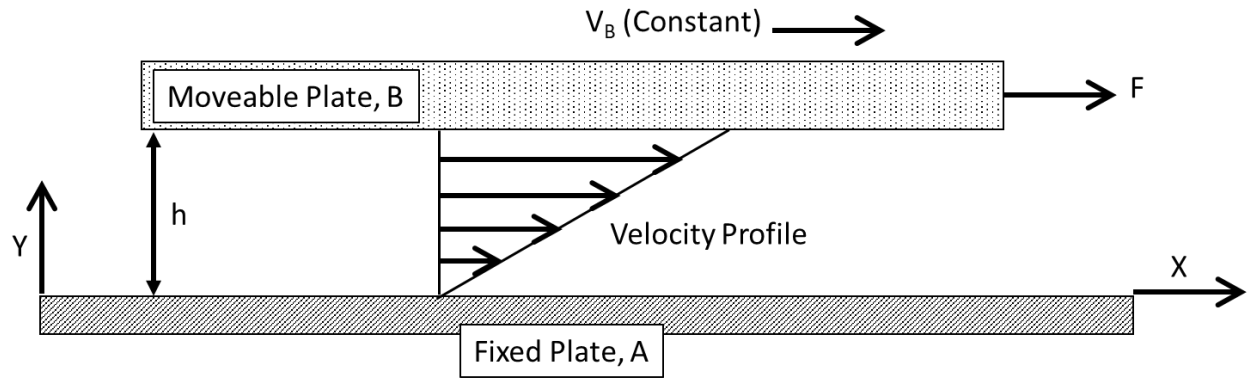

Figure 1-1*. Velocity profile of a fluid between two infinite parallel plates with a movable plate* [10].

For simple fluids, the relationship between the viscous shear stress and rate of shear strain is linear and these fluids are known as Newtonian fluids while fluids that do not follow the ideal linear relationship are non-Newtonian fluids. This ratio between the shear stress and rate of shear strain is the fluid's viscosity. For the cases of non-Newtonian fluid, the apparent viscosity is the instantaneous slope of the shear stress and rate of shear and is dependent on the shear rate in contrast to the constant viscosity of Newtonian fluids. A plot of the shear stress as a function of the rate of shear is represented in Figure 1-2 for various types of fluids. There are several different classes of non-Newtonian fluids such as shear-thickening fluids, shear-thinning fluids, thixotropic fluids, rheopectic fluids, and Bingham plastics [6, 10].

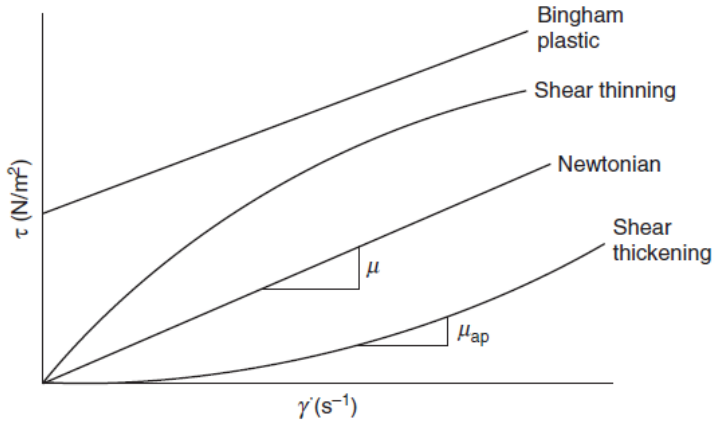

Figure 1-2. *Shear stress versus shear rate for different types of non-Newtonian fluids* [10].

There are several different methods of measuring the rheological properties of a fluid each with advantages and disadvantages. For bulk measurement of the macroscopic properties of fluids, there are standardized rheological methods such as rotational and capillary viscometers [11]. These methods typically have significant limitations when applied to samples sizes that are in the magnitude of microliters. To deal with measurement of rheological properties at micro sample size, micro-rheology methods such as optical viscometers have been developed [12].

Rheological properties of blood such as its non-Newtonian shear thinning characteristic has been known through studies using classical rheological methods such as rotational viscometers and small glass capillaries [3]–[5]. However, measurements made using standard rheological measurements to obtain intrinsic properties of complex fluids such as blood, do not represent complex fluids well since the viscosity derived from the torque measurement assumes the velocity profile is linear. The velocity profile for a simple and complex fluid is depicted in Figure 1-3. For blood the velocity profile is non-linear due to the heterogeneity of the RBC distribution caused by the formation of RBC aggregates at low shear and the formation of a CFL, which are discussed in Section 1.2.2.2 and Section 1.2.2.3, respectively.

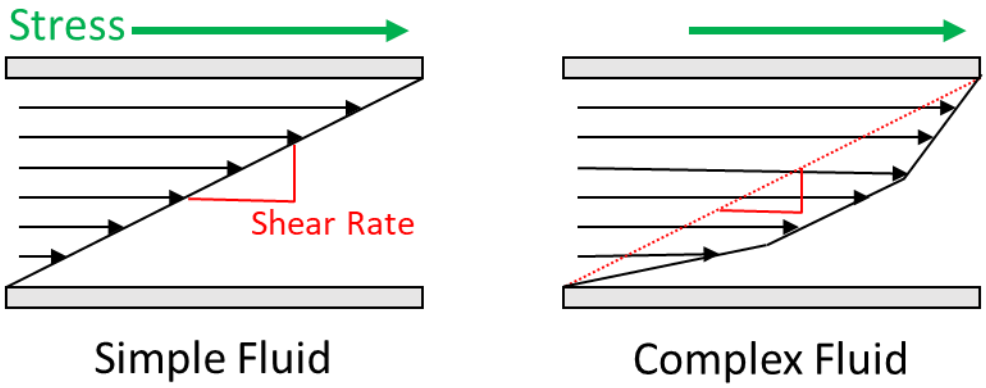

Figure 1-3*. Velocity profile for complex fluid may vastly differ from the linear profile expected for Newtonian fluids and the base assumption used to obtain viscosity in rheometers.*

1.2.2.1.1 Plasma

Plasma viscosity ranges from 1.5 cP to 1.7 cP at room temperature [10]. The presence of proteins in plasma results in the inherent higher viscosity of plasma in comparison to that of water. Experimentally, plasma is seen to behave like a non-Newtonian fluid when tested using capillary and rotating viscometer. While other studies published have suggested plasma behaves like a Newtonian fluid. However, variability in factors such as protein concentration in samples within the species, across species and experimental techniques are several possible contributing factors that results in contradictory information. Furthermore, rheological characteristics of plasma in a pathological condition may contribute to the non-Newtonian behaviour observed. Another factor that has significant influence on plasma viscosity is temperature, in which the viscosity of plasma decreases as the temperature increases [6, 10].

1.2.2.1.2 Whole Blood

In contrast to plasma, whole blood has been experimentally shown to have non-linear behaviour at low shear rates with a typical apparent viscosity ranging between 3 cP to 6 cP [6, 10]. Variation of the apparent viscosity of blood is dependent on the rate of shear strain, sample HT, temperature, cell deformability, and vessel diameter. The relative viscosity of blood is presented under various conditions in a study by Chien in Figure 1-4 [3].

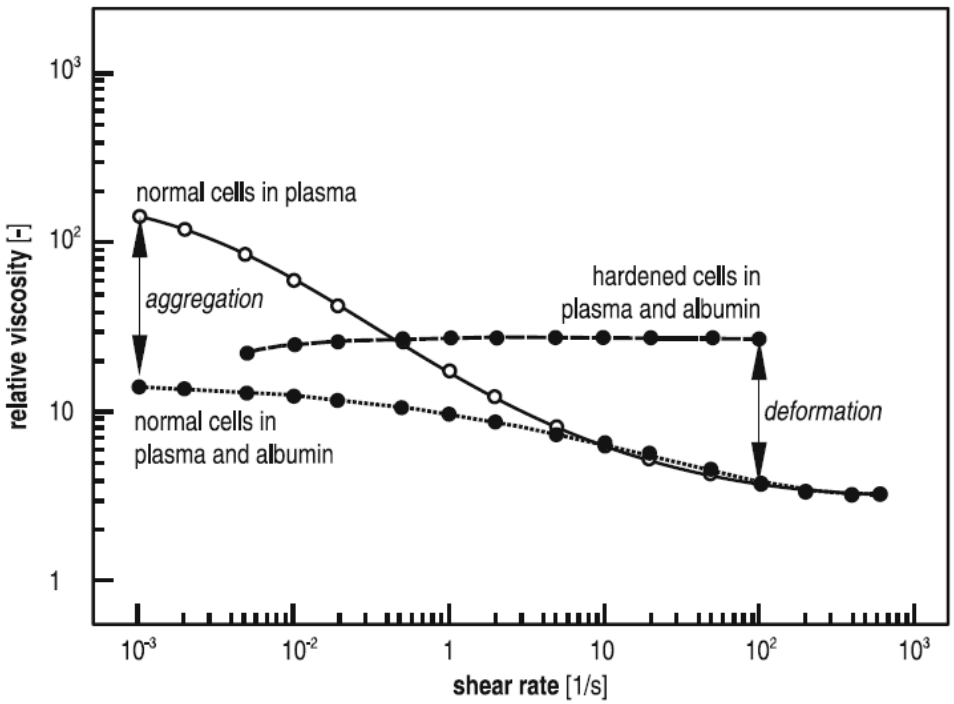

Figure 1-4. *Shear rate vs. blood viscosity data, normalized with plasma viscosity of 1.2(10^3) Pa*s for blood 45% HT* [3, 13].

When whole blood is tested under low rate of shear conditions, the apparent viscosity increases to a relatively large magnitude. This is attributed to the fact that RBC tends to aggregate into stacks known as Rouleaux formations at low shear rates. When increasing the rate of shear on blood, the stack aggregate gradually breaks up above a rate of shear of about 50 s^{-1} and for shear greater than 100 s^{-1} the viscosity approaches an asymptotic value of about 3.5 cP in which blood behaves like a Newtonian fluid [6, 10]. When completing viscosity measurement of blood, it is important to consider the rate of shear at which the viscosity measurements are obtained. With increase in HT the viscosity of whole blood also increases while also maintaining the decrease in viscosity at higher shear rate when the cells disaggregate [6, 10]. However, the viscosity of a similar HT suspension with rigid spheres results in a faster rise in viscosity than that of blood. Indicating that the deformability of cells has the effect of reducing the viscosity of blood [6, 14]. The effect of HT on viscosity measurement is depicted in Figure 1-5.

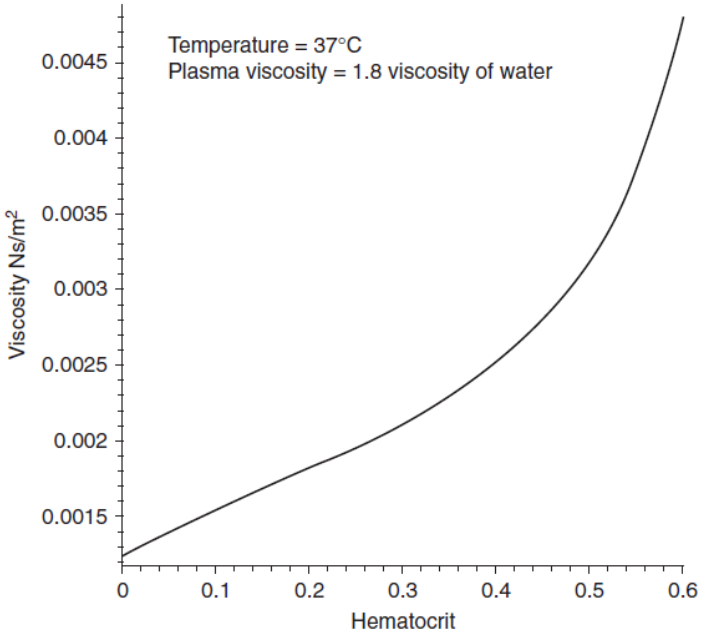

Figure 1-5*. Viscosity as a function of HT for whole blood* [10].

Apparent viscosity for blood in very small diameter tubes is very low and the viscosity increases with increase in tube diameter, which approaches an asymptotic value for tube diameters larger than 0.5 mm. The phenomenon of a decrease in the apparent viscosity in smaller tubes is referred to as the Fåhræus-Lindqvist effect. The Fåhræus-Lindqvist effect can be explained by the fact that the RBC tendency to migrate away from the vessel walls [1, 6, 15]. The resulting phenomena is a core of RBC at the center of the tube and a CFL or cell-depleted layer at the wall which is further discussed in Section 1.2.2.3. The effect of a CFL is more apparent with small diameter tubes since the cross-sectional area of the cell free zone is comparable to the core of RBC. The CFL has a lower viscosity, which is that of only plasma, lowers the apparent viscosity of the flow through the tube. In contrast, as the diameter of the tube increases the effect of the CFL diminishes hence the apparent viscosity approaches an asymptotic value [1, 6]. The effect of the tube diameter on the apparent viscosity is represented in Figure 1-6.

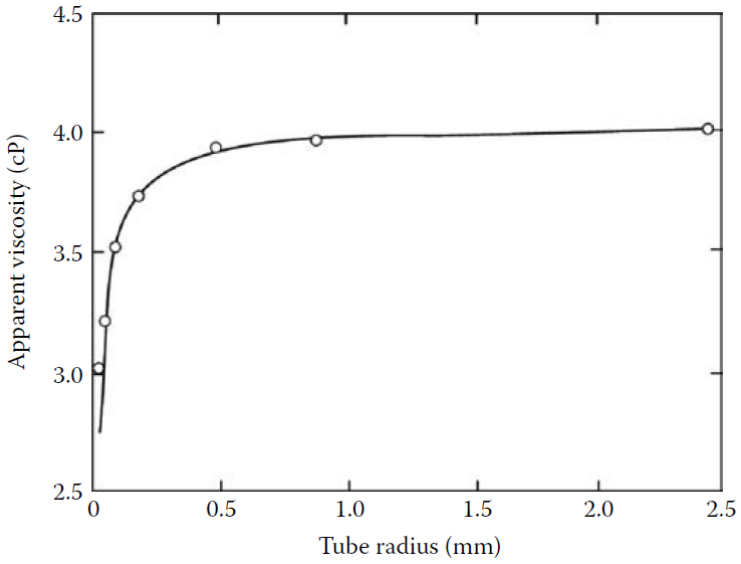

Figure 1-6. *Apparent viscosity of blood at 40% HT as a function of tube radius* [6].

1.2.2.2 Aggregation

Under low shear condition and in the presence of certain macromolecules, the phenomena of RBC aggregation occur in human blood where RBC aggregate into linear arrays, commonly known as rouleaux, or three dimensional aggregates [4]. Aggregation of RBC is a reversible process, whereby disaggregation occurs under the influence of increasing shear stress. RBC aggregation is the major determinant of the shear thinning property of blood and the other factor being the cells deformability [4]. Furthermore, studies of the RBC aggregation in a tube flow have shown complex relation between local viscosity of RBC aggregate and increase in the CFL thickness [16]. Although increase in aggregation can create blunt velocity profile which results in an increased apparent viscosity, it also can lead to greater axial migration of the cells resulting in a larger CFL at the wall which has the opposite effect [4].

The molecular model that explains the formation of aggregate is the bridging model and the depletion model. The bridging model proposed by Chien and Jan [17] describes the formation of aggregates due to the adsorption of long chain macromolecules, such as fibrinogen or dextran, onto cell surfaces which leads to bridging effect between cells [18]. Another model is the depletion model, which proposed that reduction of macromolecules concentration around RBC lowers the osmotic forces around the cells. The resulting

force causes fluid to move away and increases the tendency for cells to stick together [19, 20]. Aggregate configuration depends on several local conditions such as the shear rate and HT, and can have a variety of complex forms from the single or branching rouleaux to spheroids [18].

1.2.2.3 Cell-Free Layer

When blood flows through micro-vessels, there is a tendency for the RBC to migrate away from the vessel walls and towards the center. The migration of the cell results in two phases in the vessel, at the center there is a core of RBC while at the wall there is a cell depleted layer or cell free layer (CFL). Figure 1-7 depicts the CFL in a rectangular polydimethylsiloxane (PDMS) channel, the thickness of the layer is defined as the distance between the vessel wall and the core of RBC. This formation results in a reduction in the resistance to the flow relative to the expected resistance based on the bulk viscosity of blood [1]. There are several phenomena that contribute to the radial distribution of RBC and the formation of the CFL. It is hypothesized that the width of the CFL is due to the net contribution of the cell-wall interaction that results in radial migration to the center of the channel and the cell-cell interactions that results in radial migration to the walls.

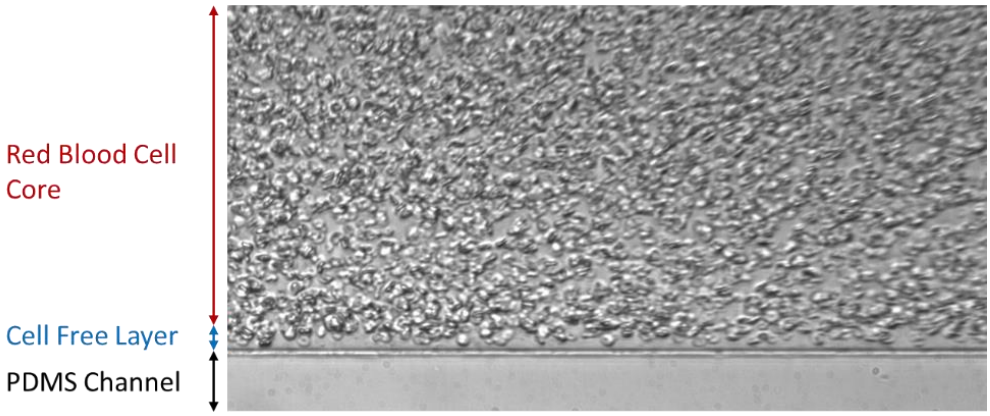

Figure 1-7. *Cell free layer and RBC core in a wide rectangular channel.*

When a neutrally buoyant rigid suspended particle is flowing through a straight channel, there are lateral forces acting upon it that results in perpendicular motion of the particle to the direction of flow. The four lateral forces include: Magnus force, Saffman force, shear gradient lift force and wall lift force. Among

them, shear gradient lift force and wall lift force are counteracting effects that dominate the lateral migration of particles and results in a equilibrium position of particles between the center of the channel and the wall [21]. However, the deformability of RBC induces additional lift forces that shifts the migration of cells away from solid boundaries moving the equilibrium point closer to the center of the channel in contrast to an equivalent rigid particle [21, 22]. Although the migration of the RBC and other deformable particles in shear flow near solid boundaries have been modelled using three-dimensional simulations, the exact mechanism of the phenomena is still being proved [1, 23, 24]. Another factor that contributes to the migration of the RBC is due to the curvature of the velocity profile in tube flow. In a numerical study by Kaoui *et al.* [25], it was found that when a vesicle is placed in an unbounded Poiseuille flow there is a cross-streamline migration of the vesicle toward the center of the flow due to interactions between the non-linear character of the flow and the vesicle deformation.

The shear flow and velocity curvature are mechanisms that lead to the formation of a CFL and would cause RBC to be driven to the center of the channel in dilute suspensions. However, at physiological conditions, the inward radial migration is opposed by the effect of RBC crowding the centerline of the channel [1, 22, 26]. In shear flow of a concentrated suspension, the frequency of cell to cell interaction or collision results in the migration away from regions of high concentration of cells at the core to lower concentration of cells at the vessel wall. This effect is termed as shear-induced diffusion or dispersion [1, 27]. A schematic of the cell-cell and cell-wall interaction is represented in Figure 1-8.

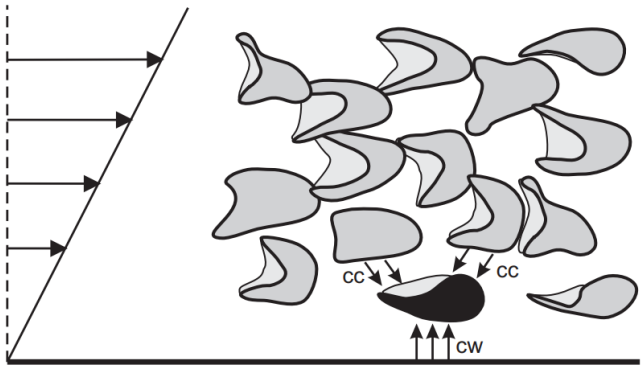

Figure 1-8. *Schematic diagram of the force balance between cell-cell (CC) interaction and cell-wall (CW) interaction resulting in a net lateral force acting on the cell* [28].

As discussed in Section 1.2.2.1.2, the presence of the CFL near the wall results in a substantial reduction in flow resistance. In the glass capillary viscometer experiment from Fåhræus and Lindqvist [5], it was found that the viscosity of blood in cylindrical channels smaller than 300 μm could not be accurately determined using Poiseuille law due to the significant effect of the CFL. The effect on the apparent viscosity is significantly affected by the CFL if it is considerably large relative to the vessel wall since the viscosity of plasma is less than that of the RBC core. Furthermore, a consequence of the RBC migration away from the vessel wall results in what is known as the Fåhræus effect, where the HT in the channel is less than the HT discharged from the channel. Since RBC is concentrated at the center of the channel, it travels on average faster than the surrounding plasma in the CFL and has a shorter time to reach the end of the channel [1]. Several factors affect the thickness of the CFL such as the channel dimensions, HT, shear rate, aggregation, and cell deformability.

1.2.3 Rate of Shear Strain

Rate of shear strain, $\dot{\gamma}$, is an important parameter that influences RBC aggregation and deformation, which results in changes in the formation of the CFL and therefore apparent viscosity. The rate of shear strain is defined as the incremental change of the flow velocity and incremental distance change perpendicular to the direction of shear stress [6, 10]. This is represented by Equation (1),

$$\dot{\gamma} = \frac{\partial u}{\partial y} \tag{1}$$

Where u is the velocity in the flow direction and y is the incremental distance change between fluid layers. When a fluid flows through a channel, the velocity of the fluid at the wall is zero and reaches the maximum value at the center of the vessel, which results in a maximum rate of shear strain occurring at the wall and minimum at the center of the vessel [6, 10].

In vivo, the rate of shear applied on the fluid is higher in the smaller vessels such as the arterioles with mean rate of shear of 8,000 s^{-1}, and lower in the larger vena cava with mean rate of shear of 100 s^{-1} [13, 29]. It is

important that the range of rate of shear used in *in vitro* studies matches the physiological ranges to ensure that the flow condition is close to those found *in vivo*. Avoiding long exposure to significant shear stress is essential in preventing damages to the RBC and activation of platelets [6]. Furthermore, as discussed in Section 1.2.2.2, aggregation of RBC occurs in conditions of low rate shear strain which results in an increase in apparent viscosity. While an increase in the rate of shear strain disaggregates RBC and decreases the apparent viscosity of the bulk fluid.

To estimate the rate of shear strain experienced by the fluid, it can be calculated from the velocity profile obtained through micro-particle image velocimetry or fluorescence correlation spectroscopy. To approximate the rate of shear strain close to the wall, the simplest interpolation method is to assume a linear velocity distribution between the zero velocity at the wall and a single measurement point away from the wall [30]. However, Anastasiou *et al.*, suggests that two preferably three velocity values obtained near the vessel wall is used, which is represented in Figure 1-9 [30].

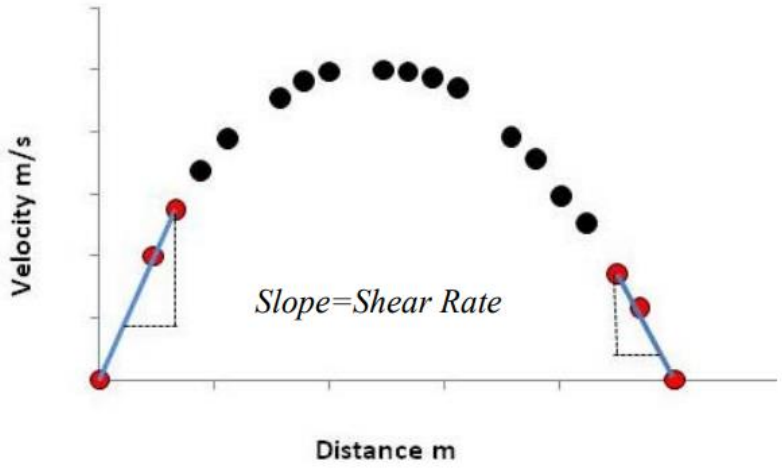

Figure 1-9. *Estimation of wall shear rate from measured velocity profile* [30].

1.2.4 Velocity Profile in Microfluidic Devices

The following section will explore the analytical and approximated equations of the single fluid flowing system through a rectangular cross-section and the analytical approximation of Couette flow system.

1.2.4.1 Single Fluid System

Having a theoretical velocity profile is essential to compare and verify experimental results. For pressure-driven flow, also commonly known as Poiseuille flow, there are analytical solutions for several commonly encountered channel geometries found in microfluidics. A common geometry used in microfluidic devices is the rectangular channel profile. A schematic of a rectangular channel is represented in Figure 1-10.

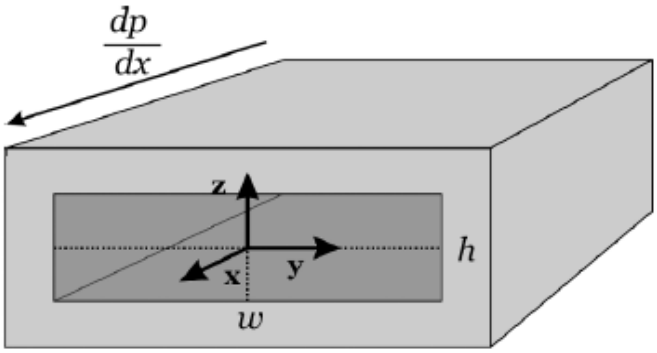

Figure 1-10. *Cartesian coordinate system for deriving Poiseuille flow profile for a rectangular channel cross-section with applied pressure gradient, dp/dx* [31].

For rectangular cross-sectional channels, the exact solution requires Fourier series to represent the velocity profile and is given by the following formulation when the coordinate is taken as the center of the channel [31] :

$$V_x(y,z) = -\frac{4\,h^3}{\mu\,\pi^3}\frac{dp}{dx}\sum_{n=0}^{\infty}(-1)^n\frac{1}{(2n+1)^3}\left(1-\frac{cosh\left((2n+1)\pi\frac{y}{h}\right)}{cosh\left((2n+1)\pi\frac{w}{2h}\right)}\right)cos\left((2n+1)\pi\frac{z}{h}\right) \qquad (2)$$

Where h is the height of the channel and w is the width of the channel. The flowrate in rectangular channel is given by [31] :

$$Q = -\frac{h^3 w}{12\mu}\frac{dp}{dx}\left(1-\frac{192h}{\pi^5 w}\sum_{n=0}^{\infty}\frac{1}{(2n+1)^5}tanh\left((2n+1)\pi\frac{w}{2h}\right)\right) \qquad (3)$$

A visual of the velocity profile for different channel aspect ratio is represented in Figure 1-11.

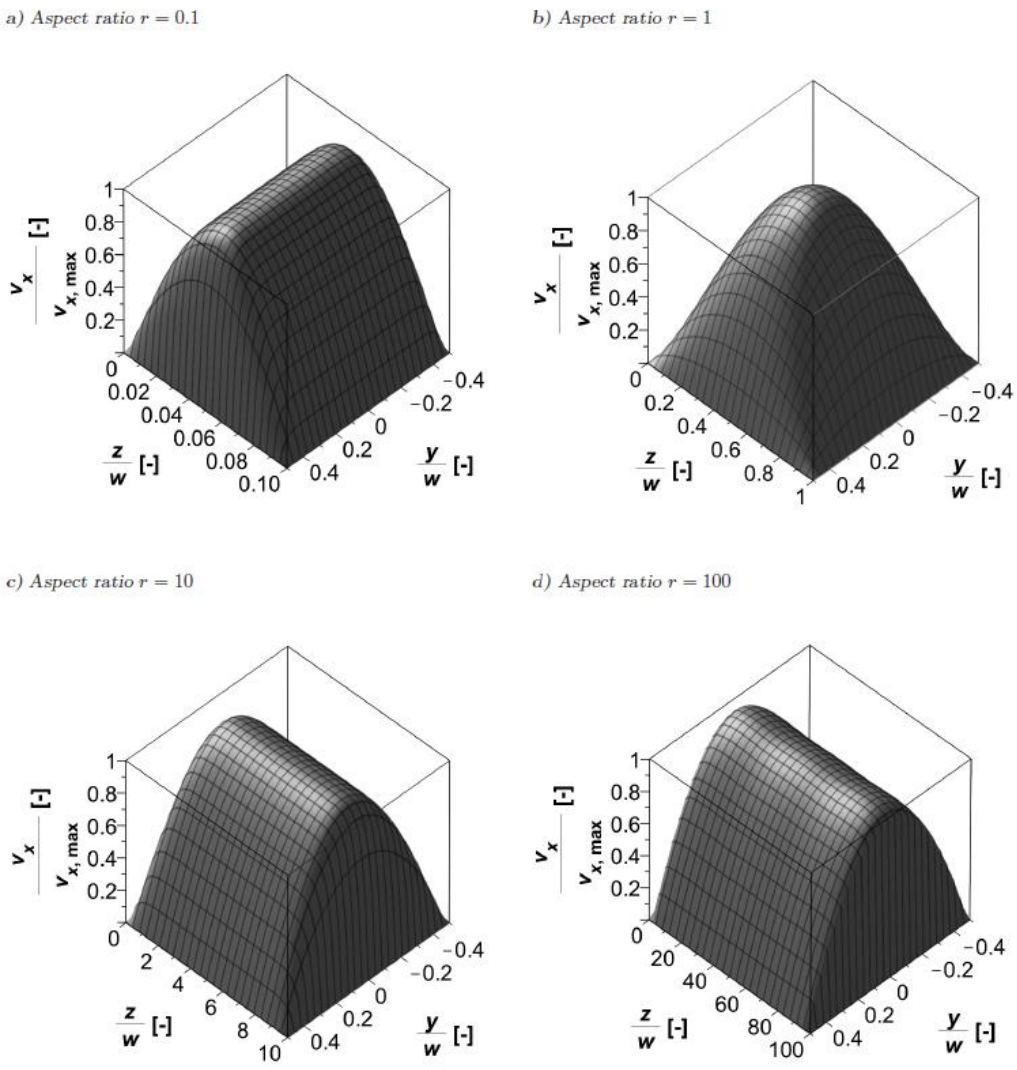

Figure 1-11. *Normalized velocity profile of rectangular channels of various aspect ratios* [31].

The velocity profile of the channel begins to approach the case of an infinitesimally elongated channel as the aspect ratio (h/w) of the channel approaches zero. An approximation of the flow rate in rectangular cross-sectional channel is given by [31] :

$$Q = -\frac{h^3 w}{12\mu}\frac{dp}{dx}(1 - 0.63\frac{h}{w}) \tag{4}$$

The error between using the exact solution in Equation (3) in comparison to Equation (4) to obtain the flow rate as a function of channel aspect ratio is summarized in Figure 1-12. It is found that the aspect ratios less than 0.65 the error in the flow rate is less than 1% and aspect ratios smaller have negligible error.

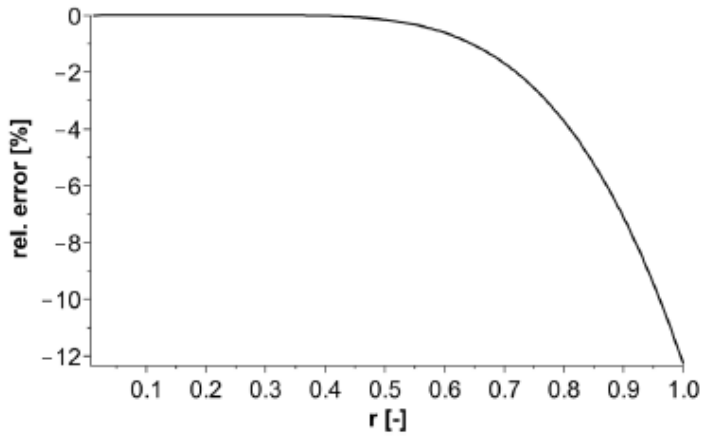

Figure 1-12*. Simplification error of flow rate using exact solution in comparison to approximation* [31].

Although the assumptions for the previous equations above are made for Newtonian fluid, they are invaluable to have to calibrate measurements made of microfluidic devices prior to the introduction of non-Newtonian fluid.

1.2.4.2 Couette Flow System

Couette flow is the flow of viscous fluids between two solid boundaries in which one is moving tangentially to the other. Section 1.2.2.1 first introduces the topic of Couette flow for its application in identifying the viscosity of the fluid of interest. The fluid is driven by the viscous forces acting on the fluid introduced by the moving interface and may be further influenced by the introduction of an applied pressure gradient. By applying the Navier Stokes equation to the two infinite plate scenario represented in Figure 1-1 of Section 1.2.2.1 in which there is no applied pressure gradient, the two-dimensional velocity profile is represented by,

$$u(y) = \left(\frac{V_b}{h}\right) y \tag{5}$$

Where $u(y)$ is the velocity profile, V_b is the velocity of the plate, h is the height of between the plate and y is the distance in the y-axis from the bottom plate. The shear rate is simply the gradient of velocity between the two plates. The advantage of using a Couette flow is that it provides a constant and controllable shear condition on the fluid, and it is the basis of some classical rheometers such as the rotating cylinder

viscometer [10]. Couette flow systems have also been incorporated into microfluidic devices as an optical viscometer method, which was first developed by Galambos and Forster [12] for estimating viscosity of Newtonian fluids. The technique is based on an analytical solution for two fluids co-flowing in a rectangular channel which is obtained using a Fourier series expansion. In a study by Mehri *et al.* [32], a two-fluid low shear rate microfluidic system was applied to RBC aggregates to measure the apparent viscosity in addition to the shear rate and aggregate size.

To approximate the velocity profile in a co-flowing system in a rectangular channel, the profile at the midplane can be modeled by assuming that it is flowing through two infinite parallel plates. The schematic is illustrated in Figure 1-13.

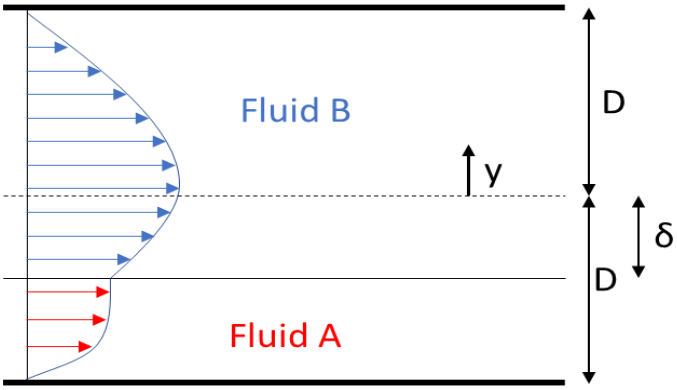

Figure 1-13. *Schematic of co-flowing fluids in an infinite plate channel, where D is the half-width of the channel and δ s the location of the fluid interface away from the channel center* [33].

By assuming that both fluids are immiscible Newtonian fluids, with the same density and fully developed the velocity profile is represented in the following equation [33],

$$u_A = \frac{1}{2\mu_A}\frac{\partial p}{\partial x}\left(y^2 + \left(\frac{(D^2-\delta^2)(\mu_B-\mu_A)}{D(\mu_B+\mu_A)+\delta(\mu_B-\mu_A)}\right)y - D^2 + D\left(\frac{(D^2-\delta^2)(\mu_B-\mu_A)}{D(\mu_B+\mu_A)+\delta(\mu_B-\mu_A)}\right)\right) \quad (6)$$

$$u_B = \frac{1}{2\mu_B}\frac{\partial p}{\partial x}\left(y^2 + \left(\frac{(D^2-\delta^2)(\mu_B-\mu_A)}{D(\mu_B+\mu_A)+\delta(\mu_B-\mu_A)}\right)y - D^2 - D\left(\frac{(D^2-\delta^2)(\mu_B-\mu_A)}{D(\mu_B+\mu_A)+\delta(\mu_B-\mu_A)}\right)\right) \quad (7)$$

Where the subscripts represent the properties of the respective fluids, u is the velocity profile, μ is the viscosity, $\partial p/\partial x$ is the applied pressure gradient, D is the half-width of the channel, and δ is the location

of the fluid interface away from the channel center. The flow rate per unit length is approximated by integrating the velocity over the width of the channel which gives the following equation [33],

$$\dot{Q}_A = \frac{1}{2\mu_A}\frac{\partial P}{\partial x}\left(\frac{1}{3}(\delta^3 - 2D^3) + \frac{C'}{2}(\delta^2 - D^2) + DC'(\delta + D) - \delta D^2\right) \quad (8)$$

$$\dot{Q}_B = \frac{1}{2\mu_B}\frac{\partial P}{\partial x}\left(-\frac{1}{3}(\delta^3 + 2D^3) + \frac{C'}{2}(D^2 - \delta^2) + DC'(\delta - D) + \delta D^2\right) \quad (9)$$

$$C' = \left(\frac{(D^2 - \delta^2)(\mu_B - \mu_A)}{D(\mu_B + \mu_A) + \delta(\mu_B - \mu_A)}\right) \quad (10)$$

With an analytical approximation of the velocity profile for the co-flow system, the applied shear rate can be approximated for a non-Newtonian fluid.

1.2.5 Velocity Measurements Technique at the Microscale

Measurement of flow fields at the microscale is important in many areas of science and engineering, with industrial applications of microfluidic devices ranging from computer to pharmaceutical industries. There are several different techniques that can be utilized to measure velocity at the microscale. The two techniques that will be discussed in the following section are micro-particle image velocimetry (μPIV) and 2-beam fluorescence cross-correlation spectroscopy (2bFCCS).

1.2.5.1 Micro-Particle Image Velocimetry

The velocity measurement technique of μPIV is a variation of the general macroscopic particle image velocimetry (PIV). Where in both PIV and μPIV, an imaging system takes images of dispersed tracing particles in the flow field at two known time instants taken in quick succession. The images of the particles are then split into subregions known as interrogation windows which are cross-correlated to determine the most likely direction of particle image displacement within the windows, a schematic of cross-correlation typically used in PIV is represented in Figure 1-14 [34]–[36]. The local velocity of the fluid within the

interrogation window is determined as the ratio of the displacement moved by the particles over the time interval between the images taken.

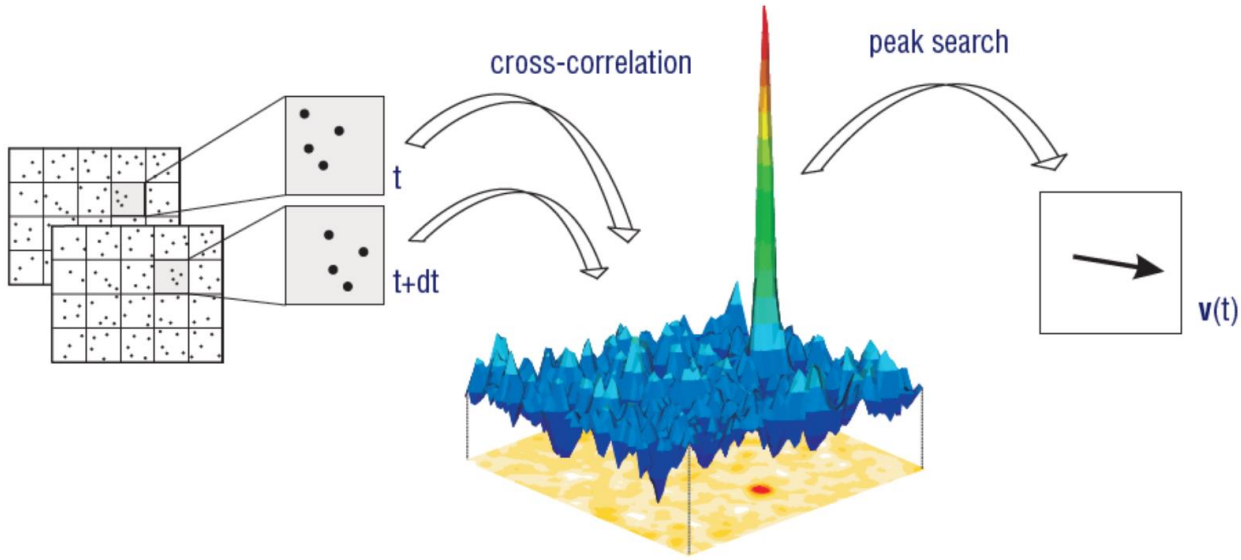

Figure 1-14. *Cross-correlation technique used in PIV to determine the position of the highest peak in the correlation plane indicating the most likely direction of displacement* [36].

The advantages of using µPIV is for its minimally intrusive, optical nature and ability to measure the whole field velocity profile with good spatial resolution. The scale of microfluidics can still be considered large enough that the fluid behaves as a continuum, however special considerations must be made for fluid forces that are often ignored at larger scales. Fluid forces scale differently at such reduced size, in which microfluidic systems commonly operate in the viscosity dominate regime, which results in systems with low Reynolds number much less than one. Other forces that are more significant on the microscopic scale include surface tension and Brownian motion [34, 35].

The key component of a µPIV system should include the microfluidic device that will be observing the fluid flow, tracing particles, an inverted microscope, a flow driving system, illumination source, light filters, and a recording device. A simplified schematic of a typical µPIV system is illustrated in Figure 1-15.

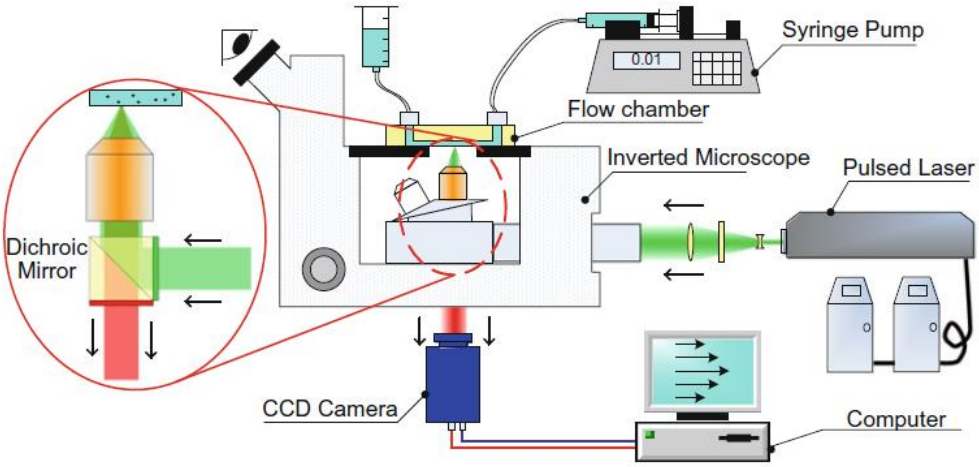

Figure 1-15. *Schematic of common 2D, planar µPIV system.* [34].

When completing a µPIV experiment, there are several equipment considerations that need to be made. From selection of tracing particles to method of illumination of the tracing particles. Furthermore, there are several considerations to make for post-processing acquired data from µPIV.

When selecting tracing particles, the size, concentration, and material needs to be considered. The size of the particle needs to be sufficiently small that the particles faithfully follow the flow and flow gradients in the device and does not change the fluid flow properties. While the particles also need to be sufficiently large that the effects of Brownian motion are minimalized [34, 35]. Furthermore, the particle density is selected such that there are no particle-particle interactions that can potentially disturb the flow or result in clogging the device and that individual particles can still be detected. Typical diameter of flow tracing particles for µPIV ranges from 200 nm to 2 µm and are usually constructed of fluorescently labelled polystyrene latex [35, 37]. To image such small particles under a microscope, a high numerical aperture, diffraction limited optics and high magnification are needed. Common objective lenses include oil-immersion lenses and air-immersion lenses.

For µPIV it is common that the microfluidic device has limited optical access to the flow. Optical access for microscopes is often limited to a single glass window in which the same window is used for both the illumination of the tracer particles and the observation of scattered light from the particles. The common

method used in µPIV to illuminate the tracer particle is through the technique of volume illumination where the whole volume of the channel is illuminated by a cone of light [34, 35, 37]. The light selection for volume illumination can either be a pulsed light source or continuous chromatic light source coupled with a gate [35]. Frequently used light sources in µPIV range from standard microscope light sources such as Hg-arc lamps to pulsed laser such as Nd: YAG lasers.

1.2.5.1.1 Limitations

Several limitations are present in µPIV that are not common in PIV. The major difference is that the particles are not considerably larger than the wavelength of the illuminated light, and the particles that are imaged using volume illumination is measured against a background of similar particles that is out of the plane of focus.

Tracing particles inside the volume illuminated will not appear as a single point in the recorded image but will form a diffraction pattern with a bright region in the center with a series of concentric rings of decreasing intensity which is commonly known as Airy disk [34]. Furthermore, all tracer particles in the flow are illuminated which results in all the particles contributing to the image taken as either discrete particles or as a background glow. Particles that are out of the focal plane of the lens contribute differently to the correlation function where particles closer to the focal plane will be observed as brighter and smaller than the particles further away from the focal plane. The measurement depth is determined by the depth of correlation defined as twice the distance that particles can be positioned in the optical plane so that the intensity is within an arbitrarily specified fraction of the focused intensity [34]. The depth of correlation accounts for the effect of diffraction, geometric optics and the size of the particles [34]. The equation for describing the theory of correlation depth was developed by Olsen and Adrian [38] and using a small angle approximation to derive the depth of correlation as [34]:

$$\delta_{Z_{corr}} = 2Z_{corr} = 2\left\{\left(\frac{1-\sqrt{\epsilon}}{\sqrt{\epsilon}}\right)\left[f^{\#2}d_p^2 + \frac{5.95(M+1)^2\lambda^2 f^{\#4}}{M^2}\right]\right\}^{\frac{1}{2}} \quad (11)$$

Where Z_{corr} is the depth of correlation, ϵ is the relative contribution of a particle displaced a distance from the focal plane, $f^{\#}$ is the focal number, d_p is the tracer particle size, M is the magnification and λ is the wavelength of the emitted light. Since the whole channel volume is illuminated, there are potential sources of error due to light scattered by out-of-focus particles which would result in flow measurements that are less spatially resolved [34].

Lastly, particle visibility is another consideration regarding illumination. Since all particles in the field of view contribute to the recorded image, the particle concentrations must be sufficiently low such that in focus particles can be imaged against out of focus particles without sacrificing on the spatial resolution [34]. The quality of μPIV velocity measurement depends on the quality of the recorded images from which the data is calculated and having images of particles that are indistinguishable from in-plane and out of plane would result in erroneous measurements.

1.2.5.1.2 Correlation Techniques

For microfluidic systems, since the Reynolds number are relatively low, the fluid mechanics' analysis mainly simplifies to quasi-steady or periodic flow. As a result, novel types of processing algorithms can be utilized such as correlation averaging. Correlation averaging or ensemble correlation is a technique that provides a more reliable estimate of mean particle displacement than standard cross-correlation as it was developed to reduce the influence of Brownian motion, low particle concentration and low-quality images that may occur in an individual image [34, 35, 39]. This is accomplished by taking a series of image pair, which are two consecutive images taking in quick succession at the same location, over a time period rather than a single paired image. Using a correlation averaging method, spurious velocity vectors can be removed as shown in Figure 1-16 to obtain an average correlation.

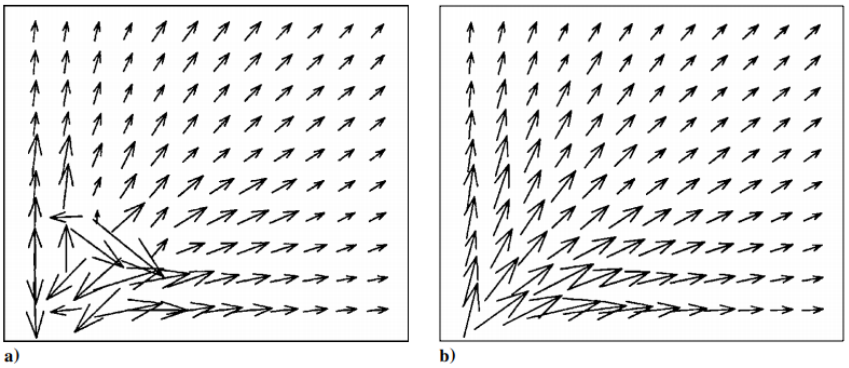

Figure 1-16. *Comparison of velocity field calculated using (a) single PIV paired image and (b) average correlation of 101 paired images* [39].

To obtain an averaged correlation function, $\bar{R}_{AB}$, an ensemble of particle image pairs is collected over a specified sample period at the same location. In Figure 1-17, multiple A and B are images taken in quick succession for an M number of repeats. Each A/B image pair is spatially correlated and the resulting correlation functions, R_n, are then averaged by the M number of image pairs. The drawback of using an averaged correlation function rather than a time instant correlation is that the instantaneous information is lost. While the advantage is the increased effective particle-image density and allows for a reduction in interrogation size, which results in a potential increase in spatial resolution [35]. A schematic description of averaged cross-correlation is represented in Figure 1-17.

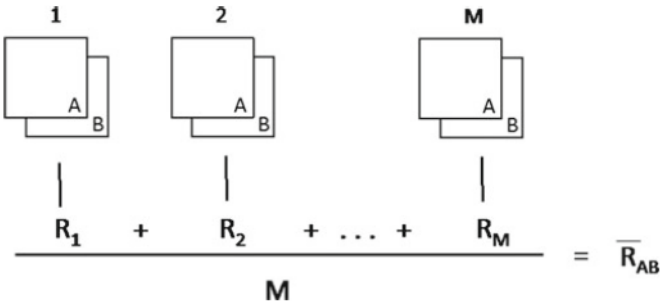

Figure 1-17. *Schematic description representing averaged cross-correlation, where A and B are images taken in quick succession, M is the number of individual image pair, R_n is the individual correlation function for each image pair and $\bar{R}_{AB}$ is the averaged correlation function* [34].

An alternative of correlation averaging is image averaging correlation, $R_{\overline{AB}}$, which is completed by making a time average of all A images and B images and then correlating the averaged image of A and B images, as indicated as $\bar{I}_A, \bar{I}_B$ averaged images in Figure 1-18. The advantage of using this technique is that it works

with low image density of fluorescence particles and is not as computationally demanding in comparison to correlation averaging [34]. A variant of image averaging was proposed by Wereley *et al.* [39] known as image overlapping, which was to produce a maximum image from a given series of paired images. The technique was then applied to µPIV by Nguyen *et al.* [40] and was shown by Pitts *et al.* [41] to be the ideal processing condition for blood micro-flows. A schematic of image averaging is represented in Figure 1-18.

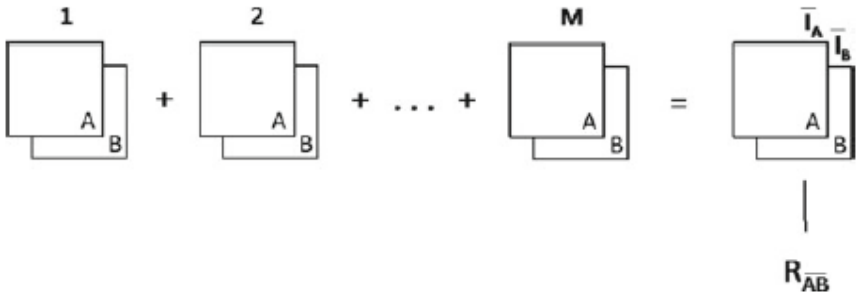

Figure 1-18. *Schematic description representing cross-correlation from image averaging, where A and B are images taken in quick succession, M is the number of individual image pair, $\bar{I}_A, \bar{I}_B$ are the averaged images, and $R_{\overline{AB}}$ is the correlation of the image averaging [34].*

1.2.5.1.3 Application of µPIV in Blood Rheology Research

The use of µPIV is a common tool to investigate flow phenomena in microchannels in the field of biological experiments and has been used to investigate blood flow both *in vivo* and *in vitro* conditions [42]–[46]. The implementation of µPIV for *in vivo* and *in vitro* conditions requires different selections of equipment and implementation considerations. For the case of *in vivo* applications, it is common that a high-speed camera is used with the naturally present RBC of the sample as the tracer particles themselves [42, 43]. While *in vitro* applications, the common method is the use of dual pulsed imaging paired with fluorescent tracer particles to determine the velocity field [45]–[47]. It is essential to understand the limitation of tracer selection in blood flow studies.

For *in vivo* applications where RBC are used as tracers or in applications where the addition of fluorescent tracers is not feasible there are several considerations to make to optimize the measurement of the velocity field. The use of RBC as the imaging tracers has its disadvantages due to the cells' size and density, which decreases the accuracy of the measurement method [40, 48, 49]. To reduce the effect of out of focus

particles and to make measurements of velocities of particles only in the focal plane, the seeding particles have to be at a low volume concentration with suggestion less than 0.1% and particle diameter should be below 1 μm [49, 50]. However, these guidelines are typically not feasible since cells' size is approximately 8 μm and physiological HT ranges from 20% to 45% between microcirculation and systemic circulation [49]. In a study by Chayer *et al.* [49] that assessed the intrinsic error of the measurement method while using RBC as tracer particles, it was found that the location of the focus plane and shape of the velocity profile has an effect of the precision of the measured flow rate. Furthermore, although RBC is not ideal at looking for the specific shape of the velocity profile, acceptable results in estimating the flow rate can be completed with measurement taken at the equatorial plane of the channel or vessel [49]. In another study by Pitts and Fenech [51], pulsed image fluorescent particles method was found to achieve a smaller depth of correlation and better representation of the velocity profile than high-speed photography using RBC. Furthermore, in the comparison, it is suggested that the pulsed methodology provides higher maximum velocity, higher shear rate and more accurate wall shear rate near the wall [51].

1.2.5.2 Two-beam Fluorescence Cross-correlation Spectroscopy

Fluorescence correlation spectroscopy (FCS) is a method that measures the dynamics of molecular process, such as particle concentration and mobility, from observing spontaneous fluorescence fluctuations induced by low concentration labelled particles travelling through a small detection volume [52]–[54]. The field of FCS has further developed with the use of confocal epi-illuminated fluorescence microscopy, and the detection and characterization of single fluorescence dye in a solution are possible for detection volume of a few femtoliters. The bases of the technique utilize an excitation laser beam that is focused using a dichroic mirror and lens to form a small confocal volume that is positioned in a cell or channel. The fluorescent molecule is excited by the laser and reemits a light that is transmitted through a dichroic mirror, band-pass filter, and a pinhole to a photodetector. The photodetector counts the photons and passes the data to a computer to complete an autocorrelation of the data either through a hardware based multi-tau real-time autocorrelator or through a software [52]. The autocorrelation analysis compares the fluorescence time

signal with itself at different times [52, 53]. These measurements are completed on systems in thermodynamic equilibrium since driving forces for spontaneous fluctuation arises from thermal energy, which causes random variation of amplitude and time in the fluorescent fluctuation [52, 54]. A sample configuration of an FCS setup is depicted in Figure 1-19.

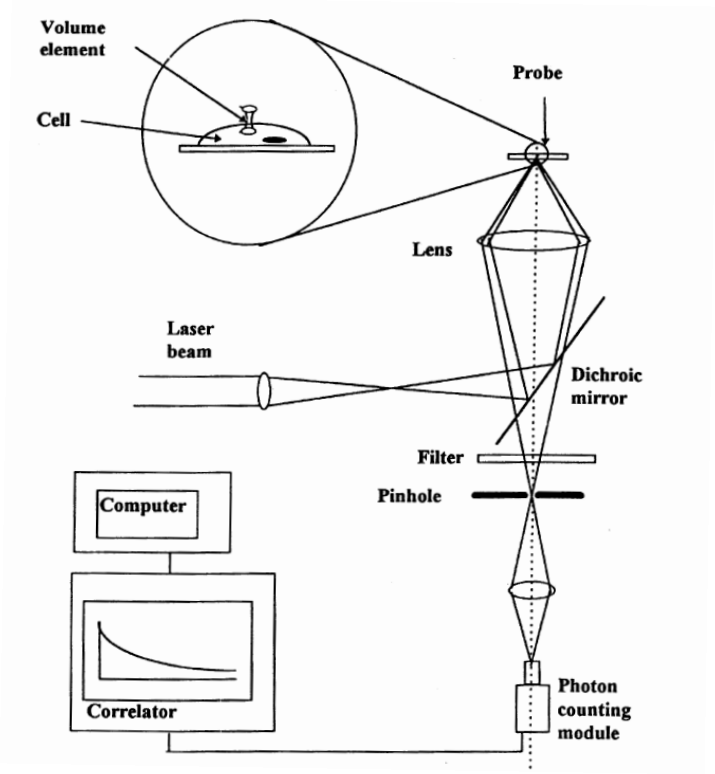

Figure 1-19*. Sample FCS schematic for experimental setup* [52].

FCS allows for indirect measurement of processes between molecules, molecular complexes and small organelles that are not typically observable using traditional microscope technique with visible lights due to limited optical resolution [53]. In addition to observing diffusion and kinetic processes, FCS is also able to complete flow analysis [52]–[55]. However, using a standard single focus FCS setup has limitations on the maximum velocity measurement of around 0.5 mm/s and identification of flow direction in the single focal volume [52, 54, 55]. To gain sensitivity to flow direction and improvement of the maximum velocity measurement, 2bFCCS can be used. For 2bFCCS, two spatially separated volume elements can be produced with a single laser with the addition of two polarized beam splitter and adjustable mirrors to generate two parallel beams. The emission from the two excited detection volumes is collected through a dichroic mirror,

filtered, and focused by an imaging lens into separate multimode glass fibres which lead to separate detectors. A sample schematic is depicted in Figure 1-20. The advantage of using 2bFCCS is that it provides a fast and easy method of determining the flow velocity ranging from 10 µm/s to 10 cm/s with reasonable detection time of 10 to 100 sec [52, 54].

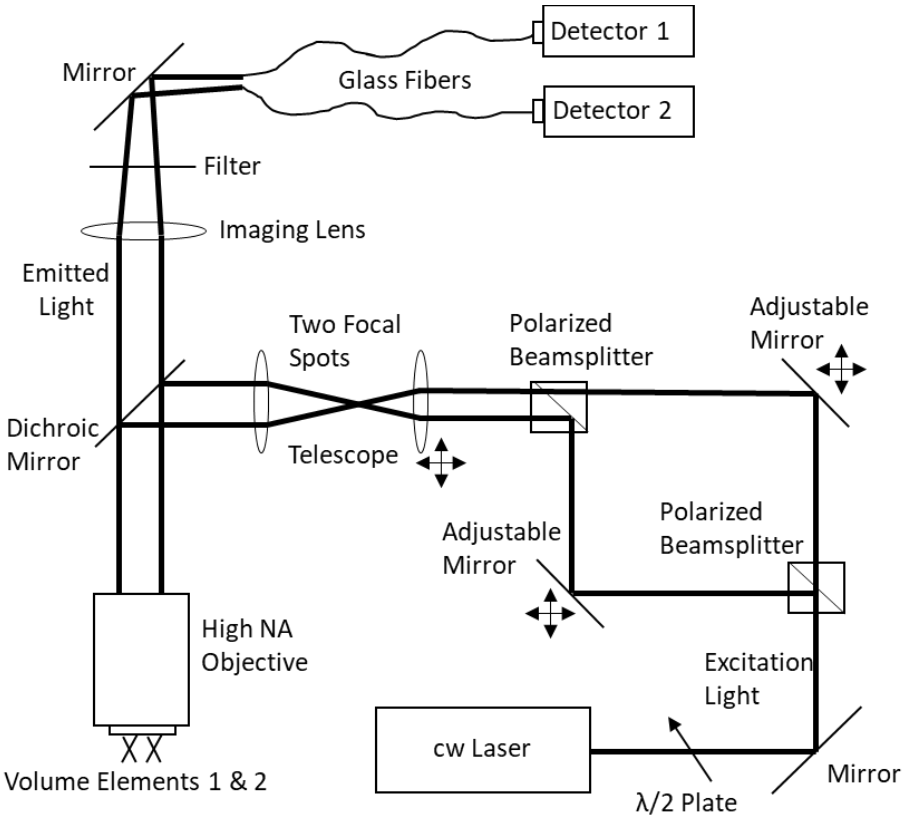

Figure 1-20. *2bFCCS schematic of experimental setup* [52].

1.2.5.2.1 Limitations

The basic components of both the FCS and 2bFCCS setup have very similar experimental setup and to determine the required detection volume size is dependent on the application, where a small detection volume is required for slowly diffusing particles while a large detection volume is suitable for fast diffusion. The detection volume also plays a role in determining the maximum fluorophore concentration that can be used since the fluctuation in the number of molecules is dependent on the detection volume [53]. To reduce error and artifact risk in FCS and 2bFCCS it is important to ensure that the fluorescence labeling does not interfere with the biological functions, and the appropriate spectral configuration must be selected such that

the effects of photobleaching, nonlinear detector response, autofluorescence background and spectral cross-talk are considered [53]. To achieve a good FCS signal, a strong fluorescent signal per labelled molecule is used if the autofluorescence background is unavoidable. The brightness of particles is dependent on the detection efficiency of the experimental setup, the specific dye used and the choice of laser for excitation. However, the maximum excitation power is limited by the dye's photostability as photobleaching of the dye needs to be avoided to avoid artifactually decreasing diffusion time and reducing cross-correlation values [53].

1.2.5.2.2 Correlation Analysis for Flow Rate Analysis

To extract the flow rate and diffusion coefficient using 2bFCCS, fluorescence intensity fluctuation caused by molecules traversing the two focal volumes are required. The normalized cross-correlation function $G_C(\tau)$ between the two-fluorescence intensity signal F_1 and F_2 from the two focal volume element V_1 and V_2, is defined as follows [54],

$$G_C(\tau) = \frac{\langle F_1(t,\vec{r})F_2(t+\tau,\vec{r}')\rangle}{\overline{F_1}\,\overline{F_2}} \tag{12}$$

Where $\vec{r} = (x, y, z)$ and $\vec{r}' = (x', y', z')$ are the spatial coordinates for the two focal volumes V_1 and V_2, respectively. The fluorescence fluctuation intensity between the two volumes is shifted from the second focal volume to the first focal volume at a time, t, by the correlation interval, τ. The cross-correlation is normalized by the product of the average fluorescence intensity $\overline{F_1}$ and $\overline{F_2}$. A more complete formulation relating the fluorescence intensity fluctuation to the molecular concentration fluctuation function and molecular fluorescence detection efficiency to obtain the concentration cross-correlation, $G_C(\tau)$, is discussed in the study by Brinkmeier *et al.* [54].

In the situation where flow in the z-direction is negligible and negligible diffusion, the cross-correlation function is simplified to [54]:

$$G_C(\tau) = \frac{1}{N}\exp\left[-\frac{R^2}{w_o^2}\left(\frac{\tau^2}{\tau_F^2} + 1 - 2\frac{\tau^2}{\tau_F^2}\cos\alpha\right)\right] \quad (13)$$

Where N is the average molecule number in the detection volume, R is the distance of the two focal volume, w_o is the radius of the volume element, τ is the shifted time between the two focal volume, τ_F is the flow time defined as the ratio between the distance between the center of the focal volume and the flow velocity. Finally, α is the angle between the direction of the flow velocity and the connecting vector of the two focal volumes. A key characteristic that is notable of Equation (13), is that the cross-correlation function increases with decreasing average molecules in the focal volume, indicating that a decrease in fluorescent concentration is beneficial in improving overall measurement. Furthermore, the cross-correlation function increases from small values of τ to a maximum values of $G_C(\tau_{max})$ at τ_{max} and then decreases to zero for very large values of τ. The maximum of the cross-correlation for zero diffusion would occur at τ_F.

1.2.5.2.3 Application of FCS in Blood Rheology Research

The use of FCS has been explored and is well suited in studies looking at molecular mobility, transport and diffusion in both *in vivo* and *in vitro* environments [52, 53]. However, the application of 2bFCCS in blood rheology and blood flow has not been fully explored. With 2bFCCS it may be possible to explore dense suspensions of RBC in both bulk flow as well as microcirculatory conditions looking at the spatial distribution of RBC and the velocity profile. In dense suspensions where the fluorescent particles may be blocked by cells, adaptation to the 2bFCCS would need to be explored. In a study by Wennmalm *et al.* [56], an alternative version of FCS is presented which explores the signal of the medium surrounding the particle is analyzed rather than the particle itself and is further adapted to 2bFCCS as well [57]. With the application of an inverse FCS or inverse FCCS, exploring different methods of label selection would be important in producing accurate measurements of velocity profiles of blood flow.

1.3 Research Statement and Objective

In collaboration between the University of Ottawa and University de Montpellier (France), the long-term goal is to couple the rheological measurement of blood flow with the characterization of local microstructures phenomena when blood flows through both simple and complex geometry. Rheological studies of blood have so far been descriptive, such as revealing the heterogeneous distribution of RBC in microcirculation, or classical, such as relating the apparent viscosity of blood to the increase in applied shear stress. By coupling rheological measurement of blood flow with local microstructure phenomena a true description of blood rheology can be developed.

For this master's thesis, the objective of this study is the development of the platform and application of tools for studying blood rheology. The two measurement tools that are explored are µPIV and 2bFCCS, in which only µPIV has been utilized to observe blood in microflow. The objectives are:

1. Development of application of µPIV analysis on a co-flow microfluidic device by characterizing velocity profile, rate of shear, and the CFL thickness of blood in microflow.
2. Development of application of two-beam fluorescence cross-correlation spectroscopy for blood rheology by verification of the fluid admissibility, the effect of laser intensity on inducing photobleaching, and the velocity measurement performance.

2 Methodology and Materials

This chapter outlines the methodology and materials used for the μPIV and 2bFCCS development by presenting the fabrication of the microfluidic devices, sample preparation for the experiments, and the flow characteristics obtained using the measurement technique.

2.1 Micro Particle Image Velocimetry

2.1.1 PDMS Channel Preparation

For the μPIV experiment, a microfluidic chip, which is a device that has a micro-channel etched or molded into the material, is used to observe the velocity profile of the fluid flowing through the channel design. Polydimethylsiloxane (PDMS), which is a clear polymer widely used in the prototyping of fabrication of microfluidic chips, is used for its optical clarity for microscopy and ease of manufacturing. The standard method of creating PDMS chips is through a process of soft lithography. This starts with the use of a master wafer with the design etched on top. The master wafer is either created on a silicon wafer through a process of photolithography or created using epoxy through a copying process [58]. For this project, an epoxy master mould is shared with another project which is produced using a PDMS-PDMS replica moulding technique to create the PDMS chips [58].

To fabricate the PDMS chips, a two-part PDMS elastomer and curing agent (Sylgard 184, Dow Corning, USA) is mixed in a 10:1 ratio under a fume hood for 5 mins until thoroughly mixed. The mixture is then placed into a vacuum chamber to complete a preliminary degassing for 30 mins in the original mixing container. Once degassed, the mixture is then poured onto the pattern mould and degassed once again for 30 – 60 min to remove any residual bubbles. The mould is then placed onto a hot plate set to 60°C for 90 min and left to dry for another 24 hours. The dried PDMS is then carefully removed from the mould avoiding any tears of the PDMS copies while using a scalpel. Inlet and outlet holes are then punched into each microchannel using a 1.0 mm diameter Miltex biopsy punch (Ted Pella Inc., USA). The surfaces of

the PDMS channels are then cleaned and sealed with clear scotch tape to prevent contamination of dust particles. Using an oxygen-plasma system (Plasma Etch, USA), each PDMS copy is bonded to a glass slide to enclose the channel with a fourth wall to form the final chip. Prior to using the PDMS chip, the channel is plasma treated through the inlet and outlet port using a plasma gun (Corona Treater, BD-20AC, Electro-Technic Products Inc) for 20 seconds to improve the surface hydrophilic properties when flowing the working fluid through it. The purpose of improving the hydrophilic surface properties of the channel is to ease the bubble removal that may occur when using the channel during experiments.

For the design of the PDMS chip used in the μPIV experiment, a co-flow channel design is used with two inlets and a singular outlet. At the two inlet branches, there are a series of pillars which has the purpose to help break up large aggregates that may form. The mean channel width is 2.05 mm ± 0.014 mm at the length of the channel where the two inlets has converged into a straight channel. The final chip design is represented in Figure 2-1.

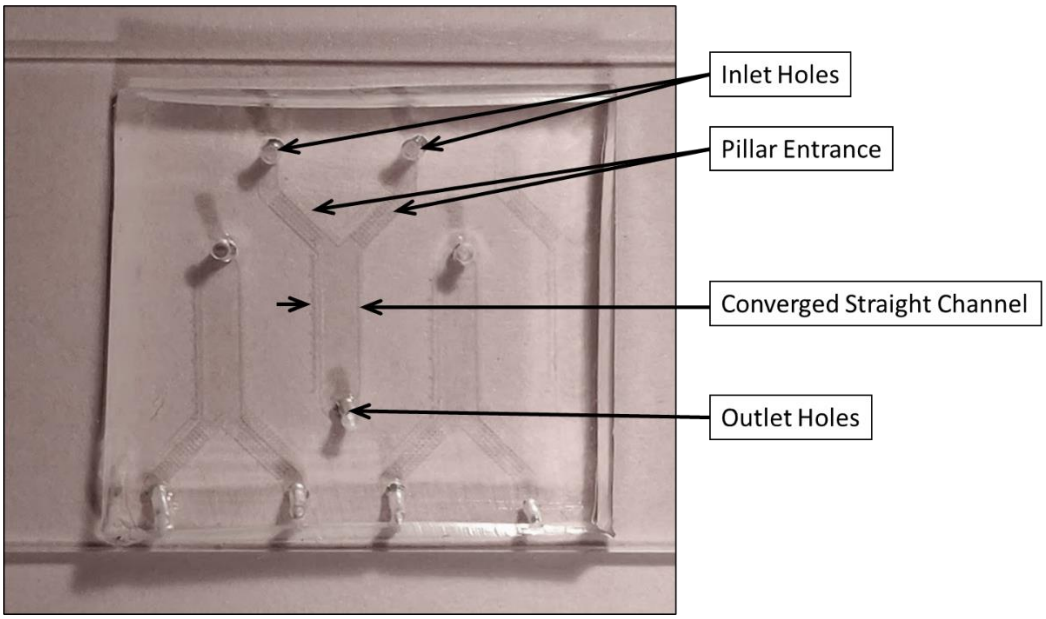

Figure 2-1. *PDMS chips used in the CFL experiments.*

2.1.2 Sample Preparation

The μPIV experiment involved the use of human blood, and phosphate buffered saline (PBS) and glycerol solution to flow in the co-flow microfluidic device. The following section will go into detail the preparation of the different sample fluids.

2.1.2.1 PBS and Glycerol Preparation

Several PBS and glycerol solutions are prepared at 0% (pure PBS), 10%, 20%, 30% and 40% glycerol to PBS by mass. To determine the appropriate solution to be used as the second fluid in the co-flow microfluidic device, glycerol. These solutions are tested for their viscosities using a commercial Viscometer (m-VROC, Rheosense Inc., USA). PBS is prepared by combining the base tablets (P4417, Sigma-Aldrich, Germany) with 200 mL of de-ionized (DI) and not distilled water using a magnetic mixer for 30 mins to make the x1 PBS solution. To make the glycerol and PBS solution, the components are then weighed using the analytical balance (SECURA224-1S, Sartorius AG, Germany) and mixed using the magnetic stirrer for 30 mins until homogenous.

2.1.2.2 Blood Sample Preparation

For the experiment, fresh and healthy blood samples are needed to be collected and prepared to complete measurements. Human blood is collected from healthy individuals with approval of the ethics committee at the University of Ottawa (ETHICS CODE H03-19-3341) and is collected at the Dynacare Laboratory and Health Services Centre with the help of accredited professionals. The blood sample is collected using 4 mL tubes which are coated with ethylenediaminetetraacetic acid (EDTA) to prevent coagulation of the whole blood during transportation. The typical total collection volume is approximately 12 ml per individual donation, and this is to ensure that there is enough sample to complete a full experiment and therefore reduce variations of measurements due to variability between blood donors.

The whole blood samples are centrifuged for a total of three times at 3,000 rpm for 10 mins. The primary objective of the centrifugation is to separate the RBC from the whole blood. The first centrifugation is used

to separate the buffy coat, which consists of the WBC and platelets, and the plasma layer from the RBC. Both the buffy coat and plasma are discarded. The buffy coat is discarded to prevent coagulation from occurring during the experiments and the plasma removed to prevent the formation of aggregation. Before the second and third centrifugation, PBS solution filtered with a 0.2 μm filter (Nylon, Non-Sterile, Fisher Scientific, Ireland) is added to the RBC and gently agitated before centrifuging. The purpose of adding more fluids and agitating the solution is to have the RBC suspended again prior to re-separating and to thoroughly remove any remaining WBC, platelets, and plasma that may still be present after the first centrifugation.

After the third centrifugation and removal of PBS, the final sample should contain only RBC. The HT is then verified by filling a capillary tube and centrifuging it in a microhematocrit centrifuge (CritSpin, Thermo Fisher Scientific Inc., China). In most cases, even after the third centrifugation the sample is not only RBC but a mixture of RBC and filtered PBS. Typical HT after the third centrifugation ranges from 80-90% HT. However, this is not a major issue as the HT measurement after the third centrifugation is then used to correct the proportions of the re-suspending fluid to bring the sample to the correct HT value.

For the μPIV experiment, the blood sample is re-suspended with a filtered PBS, OptiPrep (Sigma Aldrich, Ref. D1556) and glucose solution to bring the final sample to 10% HT. OptiPrep is introduced in addition to the filtered PBS as it acts as a density stabilizer that reduces the time it takes for the RBC to sediment due to the density variation with the suspending fluid. While glucose is added for the RBC to produce the energy through glycolysis that is required to maintain a number of vital cell functions such as the maintenance of electrolyte gradient between the suspending fluid and the RBC cytoplasm [59, 60]. The final blood sample consisted of 10% RBC, 31.5% OptiPrep and 58.5% filtered PBS, with glucose concentration 0.9 mg/ml. For the μPIV experiment, 0.79 μm fluorescent tracer particles (Fluoro-Max, Thermo Fisher Scientific Inc., USA) is mixed with the blood sample at a concentration of 30 μL/mL which emits a wavelength of emission of 612 nm and has a density of 1.05 g/cm^3.

2.1.3 Velocity Measurement

2.1.3.1 Equipment Setup Overview

A schematic of the µPIV setup is represented in Figure 2-2.

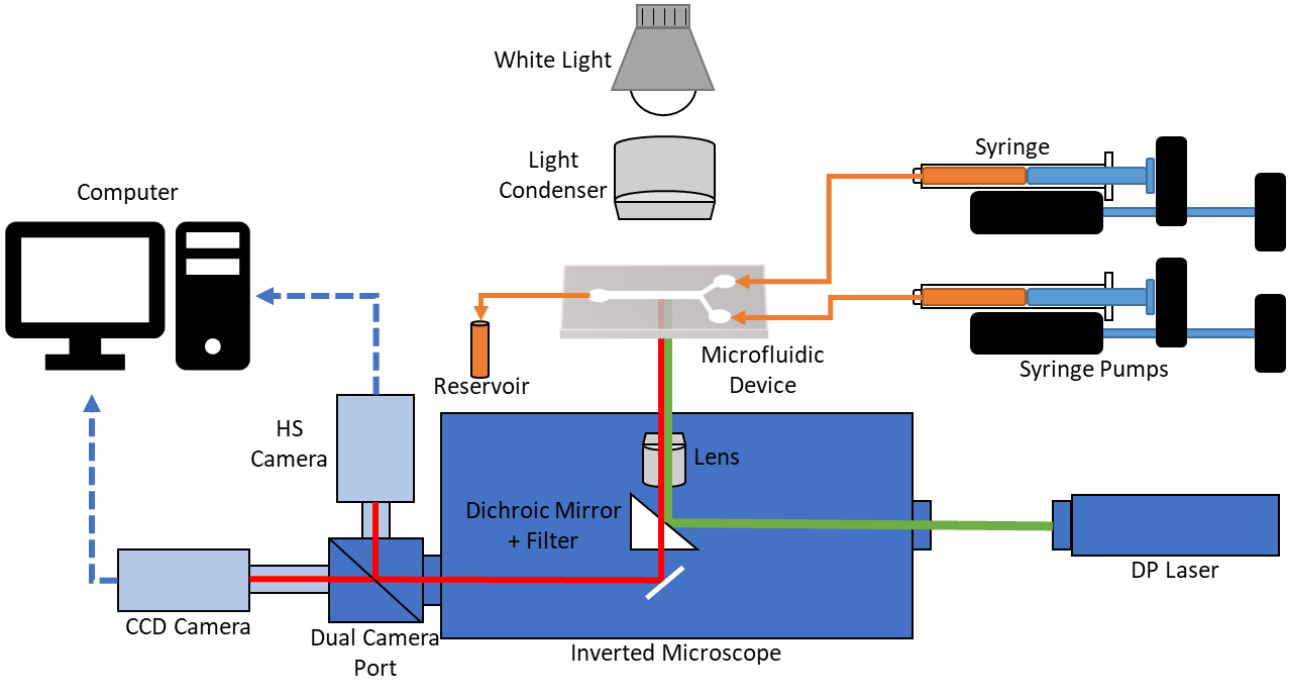

Figure 2-2. *Schematic of µPIV setup with dual pulsed laser and white light options*

The µPIV system (LaVision FlowMaster MITAS) consists of an inverted MITAS fluorescent microscope (LaVision Gmbh, Germany) equipped with a 10x (LD Plan-Neofluar, Zeiss, Germany) objective lens for a wide view of the channel. The microscope is mounted on a three-axis moveable stage, which enables measurement to be completed at any location in the microchannel with precision of up to 1 µm. The stage is controlled using the DaVis 8 (LaVision, Germany) imaging software or MITAS external controller to traverse around the channel.

The images are taken using a charged coupled device (CCD) camera (LaVision, Germany) with a Nd: YAG laser source (New Wave Research, USA) which emits a wavelength of 532 nm that excites the fluorescent tracer particles (Fluoro-Max, Thermofisher, USA). The laser timing is controlled using a programmable triggering unit that synchronize the timing of the laser trigger with the CCD camera. The laser line passes

through a filter cube which consists of a dichroic mirror and filter. The dichroic mirror directs the laser line to the device, but also only allows the wavelength of the returning emitted light from the fluorescent particles to pass through while filtering any other wavelength of light.

The emitted light from the tracer particles is then pathed to a dual-camera port that allows for the selection of the CCD camera used for µPIV or the high-speed camera (Graftek Imaging, Inc., USA) used for the CFL measurement. To control the µPIV system a dedicated computer is used that runs the DaVis 8 imaging software and contains the programmable triggering unit to time all the components together, while the high-speed camera is controlled using an adjacent computer using a LabView software (National Instruments, USA) developed by Erfan Niazi.

To control the flow in the channel, two syringe pumps (Nexus3000, Chemyx Inc, USA) system is used which is controlled through serial port connection using the PuTTy software. The software allows for control of the volume flow rate of the syringe pump independently and remotely from the pump. With the two syringe pumps, two Hamilton glass syringes (Hamilton, USA) of 1 mL and 250 µL are used and are connected to the channel using a rigid tubing and blunted syringe needle connection.

2.1.3.2 µPIV Measurements

The purpose of the microfluidic measurement is to extract the whole velocity field profile to determine the rate of shear that the blood layer is experiencing in the flow. The maximum rate of shear that the blood layer experiences occurs at the center-plane of the microfluidic channel at the channel walls. To identify the center-plane a series of velocity field measurements is taken while traversing the channel in the z-direction using the Mitas stage controller in discrete steps. The center-plane is identified when the maximum velocity of the layer peaks and begins to decrease when changing the measurement layer. With the center-plane identified, the next step is to ensure that the timing of the laser is optimal for the flow rate.

For each flow rate, the time interval between laser pulse (dt) needs to be adjusted to achieve a good cross-correlation. Ideally, the fluorescent particles travel between 5-10 pixels between the paired images and this

is affected by how fast the particles are travelling. To optimize the dt for a given flow rate, the automated dt function in the DaVis software is used which lets the user select three areas of interest to complete a calibration. For the experiment, the blood layer is used as the area of interest to obtain the optimal dt.

With the center-plane and optimal dt identified, the velocity field measurement is taken. When taking a velocity measurement for a flow rate, 100 paired images are recorded. The images are processed using a cross-correlation algorithm which determines the particle displacement between two paired images. The interrogation window size and shape are determined so that there are enough particles in the window. The correlation window starts at a size of 64x64 pixels and decreases to 24x24 pixels for subsequent passes with a window overlap of 50%. The shape of the correlation windows is oval which has a ratio of 4:1 with the longest dimension oriented in the direction of the flow and this is to improve the vector resolution from the cross-correlation. The cross-correlation is then averaged over the paired images and then averaged over the length of the channel to obtain an average 2-D velocity profile in the flow direction.

2.1.3.3 Co-Flow Planification

To plan the flow condition of the blood sample and second fluid in the co-flow channel, the analytical solution found in Section 1.2.4.2 is implemented into a MATLAB application for ease of planning. The analytical solution is taken for a fully developed flow between 2-D infinite plates of two Newtonian fluid where the fluids are immiscible and share the same density. The GUI is depicted in Figure 2-3 and provides readouts of rate of shear. The values for the base fluid, which is taken as blood, and the ratio of flow rate between the PBS and glycerol solution (Q_{PBS}) and blood sample (Q_B), and viscosity ratio is used to approximate the velocity profile and rate of shear the blood is applied.

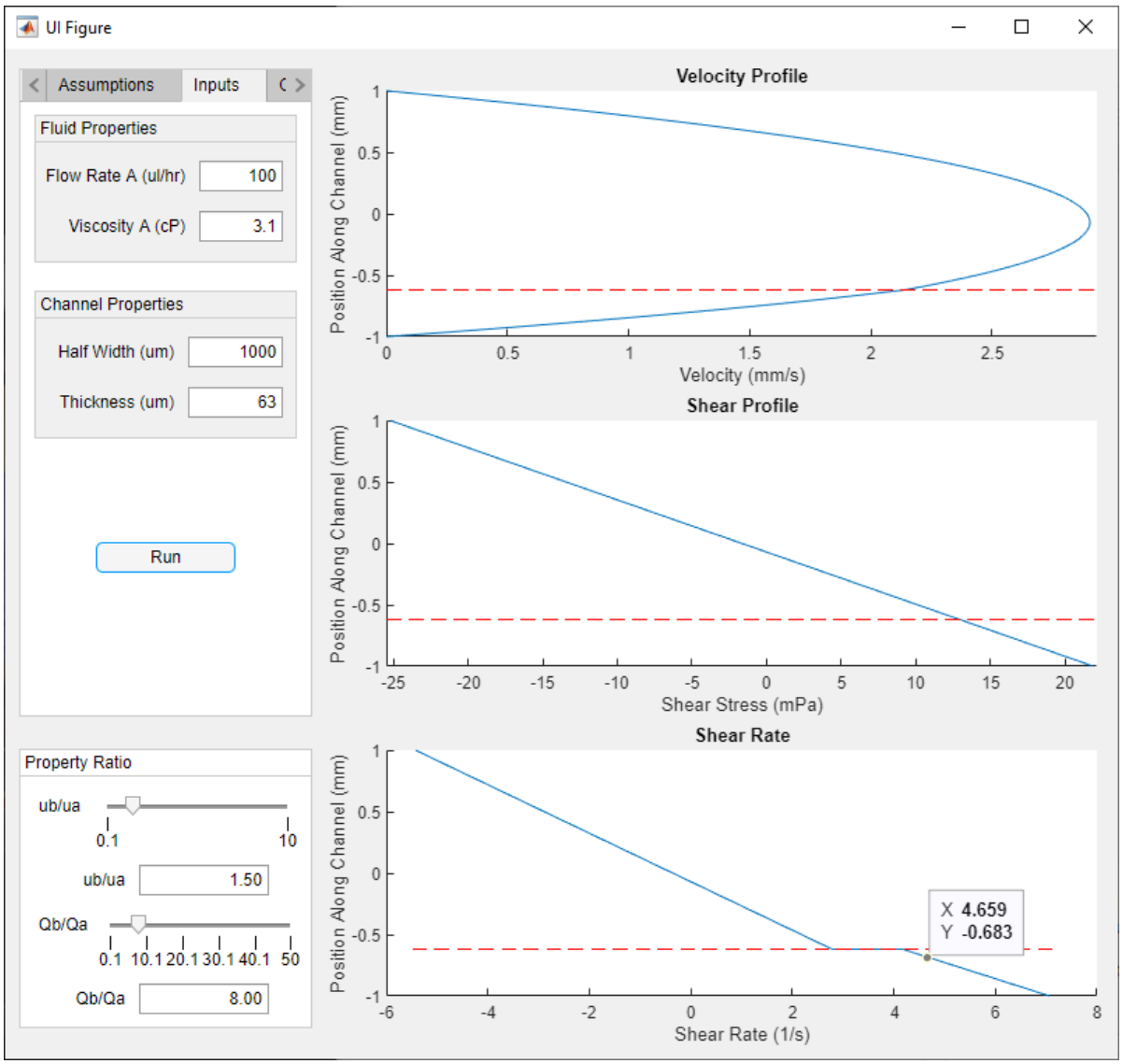

Figure 2-3. *GUI of a co-flow application built in MATLAB.*

For the experiment, the 10% HT blood sample is sheared with a 40% glycerol and PBS solution by mass. The approximated viscosity for the blood, and glycerol and PBS solution used for the approximation are taken as 2 cP and 3.1 cP, respectively. The flow conditions are outlined in Table 2-1 with the approximated mean rate of shear and the base values are taken as the flow condition for blood.

Table 2-1. *Flow rate setting used to shear blood sample*

Q_{PBS}/Q_B	***Base Flow Rate (µL/hr)***	***Approximated Mean Rate of Shear (s^{-1})***	***Blood Layer Thickness (µm)***
1	50	0.339	970
	100	0.678	970
	250	1.696	970
4	50	1.330	540
	100	2.661	540
	250	6.652	540
8	50	2.812	380
	100	5.625	380
	250	14.062	380

By changing both the base flow ratio between the two fluids and the base flow rate a range of rate of shear between 0.3 to 56 s^{-1} is achievable with the chosen flow condition. However, a larger range of rate of shear is still feasible by further increasing the base flow ratio and base flow rate. With a flow ratio of 1:25 and base flow rate of 5,000 µl/hr an estimated rate of shear of 979 s^{-1} should be achievable. It should also be noted that by increasing the flow ratio there is a shift in the location of the interface between the two working fluids which decreases the width of the blood layer.

2.1.4 Rate of Shear Analysis

From the 2-D velocity profile acquired from the µPIV measurement, the rate of shear can be determined. If the blood layer is sufficiently thin, the velocity profile of the blood layer can be approximated as being linear as approximated from the analytical co-flow model. To determine the rate of shear from the µPIV results, the location of the wall and fluid interface is identified manually by selecting the region where there are fluorescent particles as seen in Figure 2-4 (A). The rate of shear is then approximated from the velocity of the wall, taken as zero due to the no-slip condition, and the velocity of the closest point at the fluid interface Figure 2-4 (B).

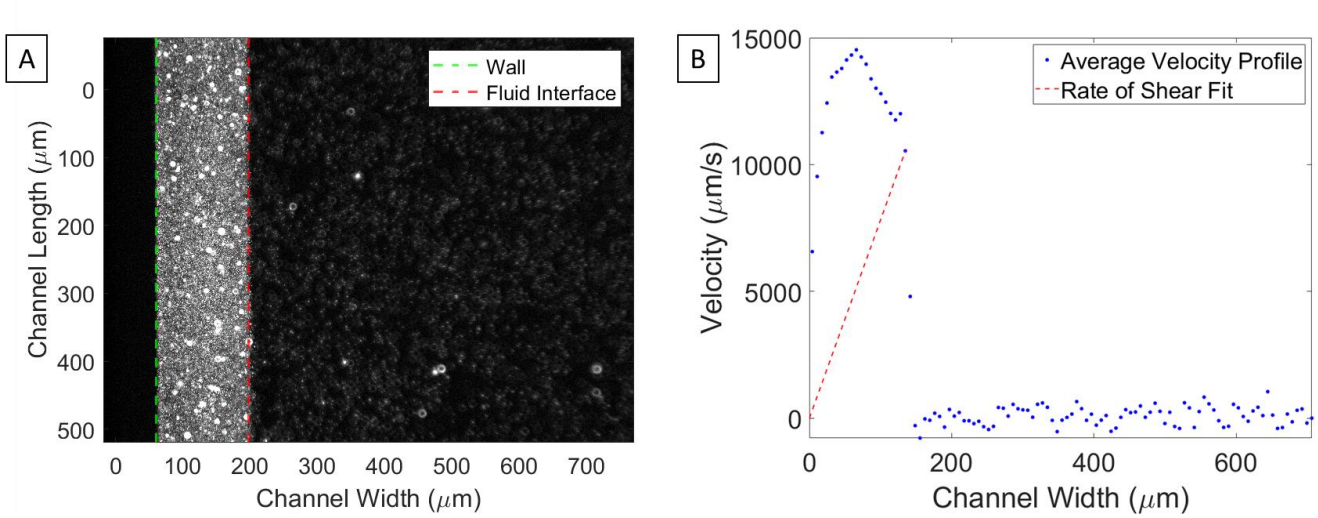

Figure 2-4. *Extracting rate of shear obtained from the velocity map. (A) The wall and fluid interface are determined by selecting the illuminated region from the fluorescent particles. (B) The rate of shear is linearly fitted to the velocity at the wall, taken as zero for the no-slip condition, and the velocity at the fluid interface.*

2.1.5 Cell-Free Layer Measurement

For the measurement of the CFL thickness, the high-speed camera is used with white light and light condenser to visualize the RBC in the channel. A 10x objective magnification is used to observe a larger portion of the flow field. The calibration of the objective lens is completed using a calibration scale, which is found to have a 2.04 pixel/µm conversion. Each image is 2040 pixels by 1080 pixels in dimension which is approximately 1,000 µm by 530 µm field of view. For each flow rate, 200 images are taken at a rate of approximately 100 fps and with a 0.1 ms exposure time. The location of the measurement of the CFL along the length of the channel is kept constant and taken at the midpoint between where the two fluids converge and the outlet of the channel.

The CFL thickness is processed on MATLAB using a modified script developed by Dr. Marianne Fenech. The script produces kymographs, which is a graphical representation of spatial position over time, of the flowing RBC and extracts the CFL thickness by identifying the distance between the channel wall and the interface where the RBC core begins. For each flow rate, up to five kymographs can be extracted with a variable pixel width. The spatial lines used for the kymographs are taken perpendicular from the direction of the flow and are dispersed along the length of the image depending on the number of kymographs to be

extracted. The same spatial lines from each time instances are extracted and truncated together to create the space vs time graph. An example of the pixel extraction and kymograph is represented in Figure 2-5.

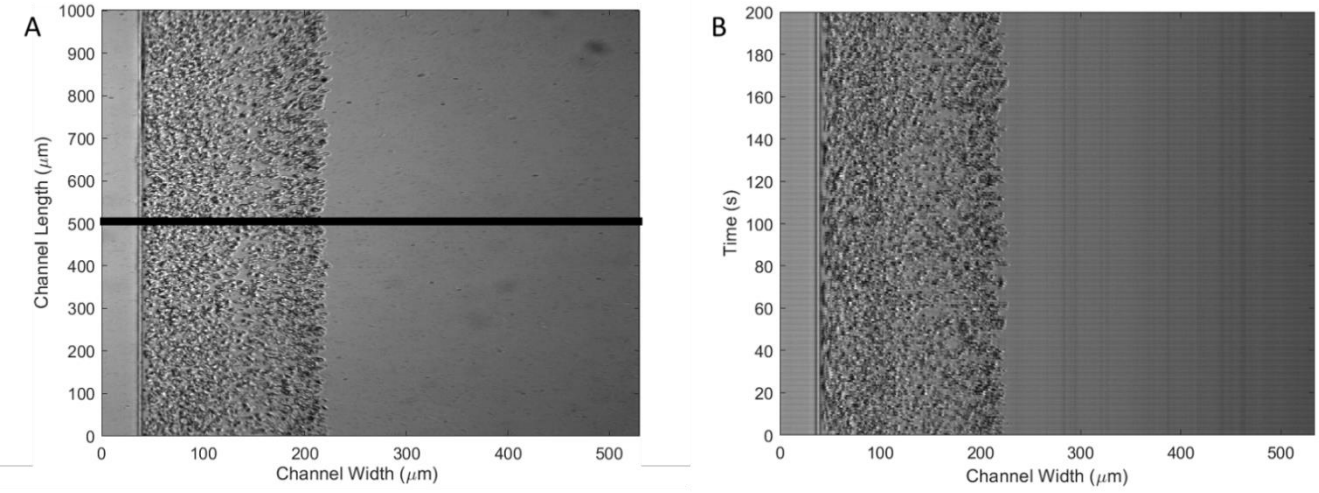

Figure 2-5. *(A) Spatial data is extracted from the same slice of the image over the 200 images recorded from the high-speed camera and an example is represented as the black line. Multiple kymographs can be made by using different slices of the recorded data. (B) A sample kymograph with 5-pixel extraction of RBC flowing through a rectangular channel.*

To extract the location of the wall and the start of the CFL automatically, the normalized gradient of the image intensity and standard deviation of the kymograph is calculated. The wall is identified where the gradient of intensity is the max since the change in image intensity is significant when moving from outside the channel wall where there is no RBC to inside the channel. While the fluid interface is determined where the intensity curve significantly decreases. In contrast, the edge of the RBC core is identified by fitting a logistic function to the standard deviation of the kymograph from the identified channel wall to the center of the blood layer. The midpoint of the logistic function is considered the start of the RBC core. With the difference between the channel wall and the location of the start of the core, the thickness of the CFL can be determined and converted from pixels to micrometres. Taking several kymographs along the length of the channel and having a wider spatial line an averaged CFL thickness is determined for a given flow rate and flow ratio configuration. An example of the intensity curve and standard deviation curve of the kymograph is represented in Figure 2-6.

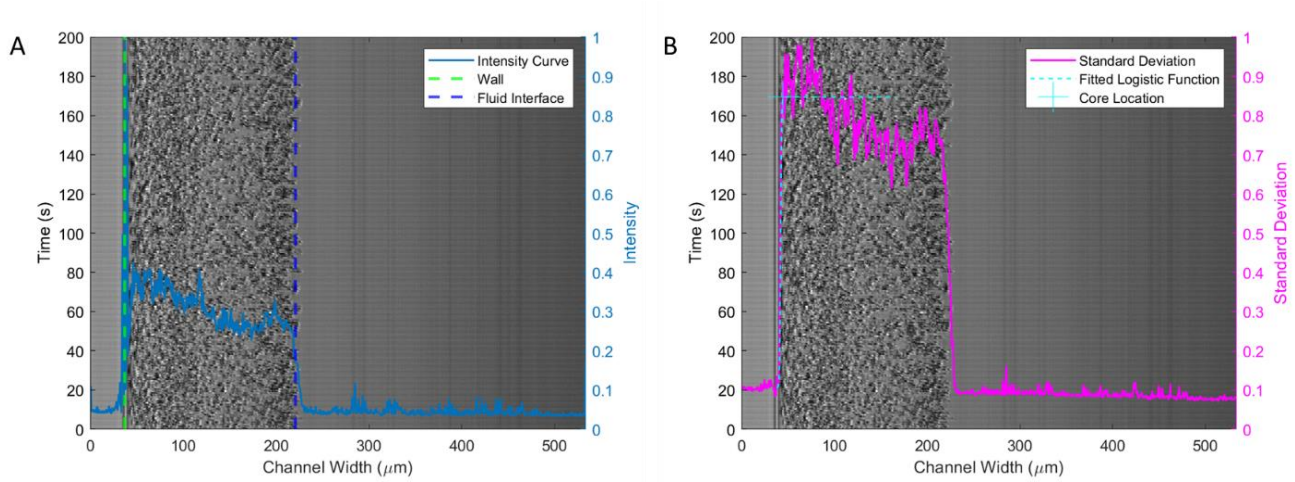

Figure 2-6. *(A) The intensity curve of the kymograph is used to determine the location of the wall and fluid interface. (B) The standard deviation curve of the kymograph is fitted with a logistic function to determine the location of the RBC core.*

2.2 Two-Beam Fluorescence Cross-correlation Spectroscopy

2.2.1 Glass Capillary Microfluidic Device Preparation

Another method of developing microfluidic devices is the use of pre-manufactured glass capillaries (CM Scientific Ltd., UK) with defined channel dimensions. These glass capillaries come in both rectangular and circular cross-sectional areas, and can be fabricated from borosilicate glass, clear fused quartz, or synthetic fused silica. The required components to convert glass capillaries into microchannels to be used in microfluidic applications include one or two glass slips (or slides), two syringe needles (20-gauge, BD PrecisionGlide Needle, BD), and quick cure epoxy. The theoretical cross-sectional view of a completed glass capillary microfluidic device is seen in Figure 2-7 in which the inlet and outlet are enclosed by the syringe needles and glass slips.

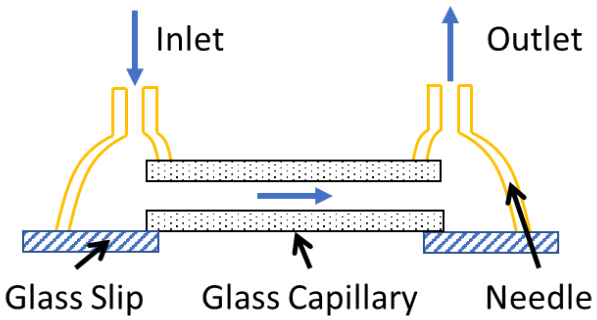

Figure 2-7. *Glass capillary microfluidic device utilizes syringe needles, glass slip and glass capillaries to create an enclosed channel. Two small reservoirs are created by epoxying the syringe needle and glass slip to the inlet and outlet of the glass capillary.*

To fabricate a glass capillary microfluidic device, the first step would be to clean and treat the glass components. Cleaning the glass slips can be completed by ultrasonicating the slips in a 1 M KOH bath for 60 min and then rinsing the slips with Milli-Q water. While for the glass capillary, the inner surface can be cleaned using a Piranha solution (a solution of 70:30 H_2SO_4 and H_2O_2), which both cleans the inner channel and prepares the surface for bonding the blocking agent Poly(L-Lysine)-PEG methyl ether (PLL-PEG). PLL-PEG is a copolymer with the PLL section being hydrophobic and PEG section being hydrophilic. The benefit of treating the surface with PLL-PEG is that it prevents the RBC from adhering to the glass capillary walls and prolonging the usage life of the microfluidic device. PLL-PEG is introduced to the surface as a HEPES and PLL-PEG solution at a concentration of 0.1 mg/mL of PLL-PEG in 10 mM of HEPES to the surface of interest and allowed to sit for at least 45 min. The capillaries can then be dried in a vacuum chamber and stored for future use.

With the glass components cleaned and treated the glass capillary can then be affixed to the glass slip or slide with a small drop of epoxy, which is to prevent slippage before the ends are capped off using syringe needles. The glass slip can either span the whole length of the channel or two slips can be used at the opening of the glass capillaries leaving the center of the channel floating between the two glass slips. The benefit of only having the slips at the entrances is that it reduces the overall glass depth that the microscope objective will have to traverse before reaching the inside channel and the fluid of interest. After the glass components have adhered to the syringe needles, which have been modified to have a small slot to account

for the glass capillary, are placed over the ends of the glass capillary and secured with more epoxy. The edges are coated with several layers of epoxy to create a watertight seal. The result is two small reservoirs made from the syringe needles that enclose the ends of the glass capillaries with the glass slips as the base. A completed glass capillary microfluidic device example is shown in Figure 2-8.

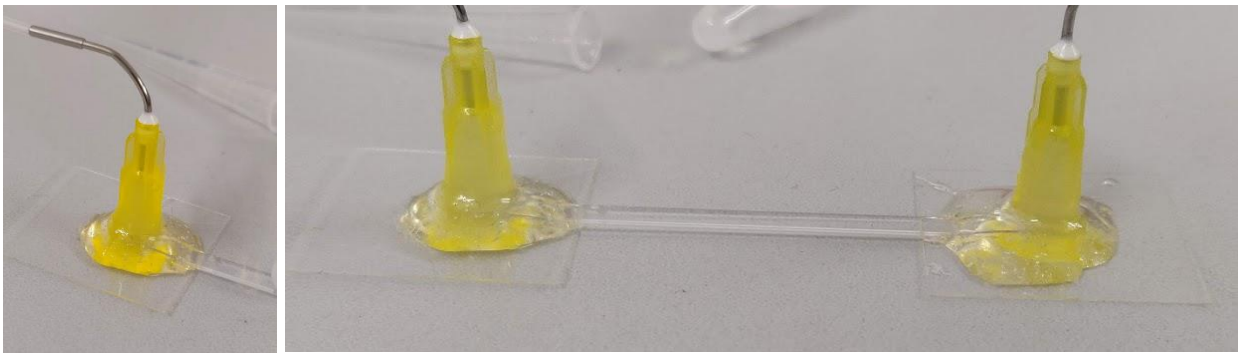

Figure 2-8. *The left image shows the syringe needle with the needle bent 90° and this is to reduce bending of the rigid tubing when using the device. The right image is a completed glass capillary microfluidic device used for the 2bFCCS experiments.*

For the 2bFCCS experiment, a borosilicate glass hollow rectangular capillary (CM Scientific Ltd., UK) with inner dimensions of 302.4 ±2.5 µm by 3.00 mm and length of 50 mm is used. For the syringe needles, a 20-gauge needle is used with the pointed ends blunted and curled to reduce bending from the connecting tube during the experiment.

2.2.2 Sample Preparation

The experiment involved the use of human blood, and Milli-Q water and fluorescent solution. The following section will go into detail the preparation of the different sample fluids.

2.2.2.1 Blood Sample Preparation

In France, venous blood samples are obtained from the local blood bank (Etablissement Francais du Sang, Montpellier, France) for the 2bFCCS experiments. The methodology for preparing blood is the same as the µPIV and is outlined in Section 2.1.2.2.

For the 2bFCCS experiment, the blood sample is similarly prepared with filtered PBS, OptiPrep and glucose solution for a HT of 10% and 40%. Furthermore, the fluorescence required for 2bFCCS is achieved by mixing fluorophore (Alexa 647, Thermo Fisher Scientific Inc., USA) at 1/1,000 the base solution which emits a max wavelength of emission of 655 nm.

2.2.2.2 Fluorescence Sample Preparation

There are three types of sample fluid scenarios that are tested: when the fluid is diluted with low concentration fluorescent molecules without any additional microparticles, when the fluid is non-fluorescent and is suspending fluorescent microparticles, and when the fluid is diluted with high concentration fluorescent molecules and is suspending non-fluorescent microparticles. Creating a fluid that is fluorescent is achieved with the use of fluorophore (Alexa 647, Thermo Fisher Scientific Inc., USA), which is a fluorescent chemical compound that can re-emit light when excited. For the fluorescent microparticles, 0.4 µm dark red FluoSpheres (Thermo Fisher Scientific Inc., USA) is used, while for the non-fluorescent microparticles 1.1 µm polystyrene beads (Sigma-Aldrich, Germany) is tested.

The normalized autocorrelation function is inversely proportional to the average number of particles contained in the focal volume. In practice to improve the correlation a very low concentration of fluorescing molecules are required to obtain reliable measurement and identifiable peak correlation time. To prepare the different dilution, a relatively high concentration of the fluorophore or microparticle is used as the base and by completing a series of step dilution the desired concentrations of the different test samples is achieved. The samples are diluted to the proper concentrations with Milli-Q water or PBS if the solution is to be mixed with blood. The fluorophore samples are diluted at 1/1,000 and 1/100,000 the base solution, while the different fluorescent and non-fluorescent particles are diluted into concentrations of 1/1,000 and 1/10 of the original concentration of 5% and 10% solids, respectively.

2.2.3 Velocity Measurement

2.2.3.1 Equipment Setup Overview

A schematic of the 2bFCCS setup is represented in Figure 2-9.

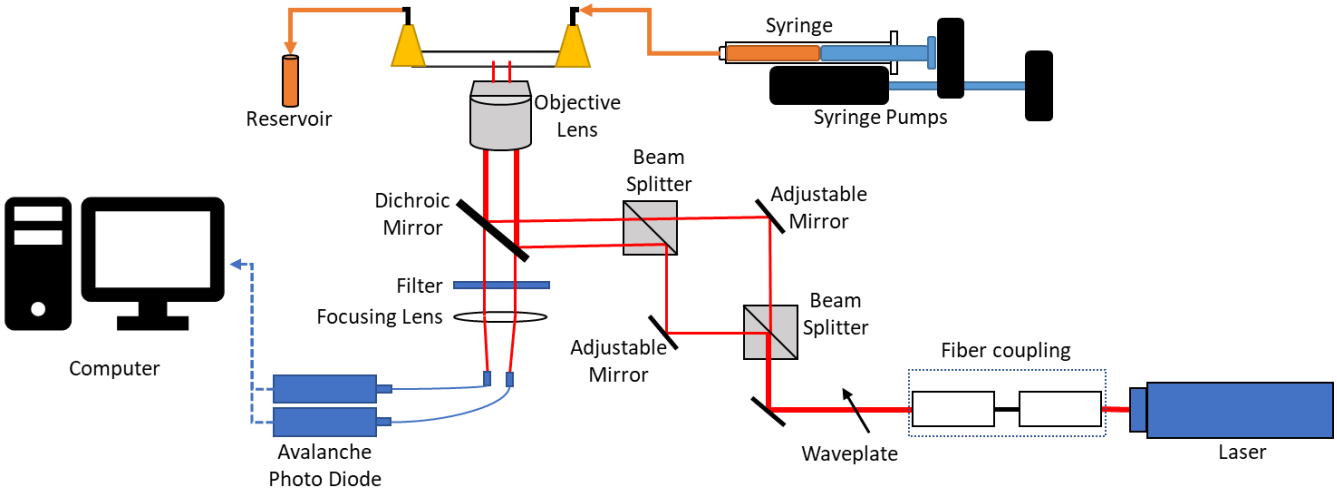

Figure 2-9. *Schematic of 2bFCCS setup*

The 2bFCCS system sits on an optical table that consists of an inverted microscope (Axio Observer A1, Carl Zeiss AG, Germany) equipped with a water immersion 63x (Objective C-Apochromat, Carl Zeiss AG, Germany) objective lens. The microfluidic device is clipped to the microscope on a three-axis manual control stage where the vertical measurement of the channel can be incremented at a rate of 2.1 µm/tick using the fine gradation. The microfluidic device or glass capillary is rotated on a slide holder (MLS203P2, Thorlabs Inc., USA) to have the two parallel beams of the 2bFCCS align oriented perpendicularly to the flow direction. This is completed manually and verified through the eyepiece of the inverted microscope. A photo is taken through the eyepiece to complete post-processing correction.

To illuminate the focal volumes for 2bFCCS a 5mW Red HeNe Laser which emits a wavelength of 633 nm is used to excite the fluorophore or fluorescent beads in the channel. The laser is primed for data acquisition by having it turned on at least an hour prior to acquisition as it was found that the laser intensity was unchanging with the digital handheld optical power and energy meter (Thorlabs Inc., USA). The laser starts

by passing through a round continuously variable neutral density filter to control the power of the laser and then condensed into an optical fibre to improve the laser signal. Control of the laser intensity is completed manually using the filter and verified with a digital handheld optical power and energy meter with a standard photodiode power sensor (Thorlabs Inc., USA) at the exit of the optical fibre.

The simultaneous generation of two parallel lasers from a single laser is accomplished with two cube polarized beam splitters. The laser passes through a waveplate prior to being split to equalize the intensities of the two beams and the positions are shifted using two kinematic mirror mounts before being coupled into the back aperture of the microscope objective. The two laser beams individually form the volume element that excites the fluorescent dye or particle. The fluorescent emission is collected through the same objective passing through a dichroic mirror, a light filter, and an imaging lens into the opening of individual fibre optics for each focal volume. The centers of the fibre optic cables are 400 μm apart and each fibre leads to an avalanche photodiode (APD) (Photon Counting Module, Excelitas Technologies Corp., USA) which counts the number of photons that are emitted from fluorescent molecule or particles that passes through the measurement volume. Data acquisition is completed using the ISS VistaVision software (ISS Medical DBA ISS Inc., USA) with the FFS module which can complete both autocorrelation and cross-correlation for FCS and 2bFCCS, respectively.

A glass capillary microfluidic device is used, and fabrication is outlined in Section 2.2.1. The flow in the channel is controlled using a syringe pump (PHD ULTRA, Harvard Apparatus, USA) with manual input of the flow condition. The working fluid is held in a 1 mL Hamilton glass syringe (Hamilton, USA) that is connected to the glass capillary microfluidic device using rigid tubing.

2.2.3.2 2bFCCS Measurements

The procedure to complete velocity measurement using the 2bFCCS setup starts with having the laser and laser system primed for data acquisition for a minimum of an hour prior to acquisition. This is to ensure that the laser intensity does not vary during data acquisition, which may affect emission fluctuation measurements. With the system primed, the measurement volume location is calibrated. This is completed

by using a standard solution of fluorescent molecules of 1/200,000 dilution on a glass slip and having the laser power at 200 µW with the focus in the drop of the standard solution. The position of the fibre optics and the adjustable mirrors are adjusted such that the photon count per second read through the ISS VistaVision software is at a maximum.

With the 2bFCCS system setup, the microfluidic device is prepared. The device is prefilled with the working fluid and any bubbles in the channel, tubing or syringe are removed prior to having the microfluidic device setup on the inverted microscope. The calibration glass slip is then replaced with the channel and secured loosely with the clip of the slide holder. The channel is then aligned to the direction of the two focal volumes manually by shifting the device position and an image is taken for future correction. The tubing attached to the channel is secured loosely to the microscope platform with tape to prevent any additional movement of the microfluidic device.

With the device secured, the different flow conditions can be tested. For each test, the syringe pump runs for at least 1 min before data acquisition between each flow condition and this is to ensure that the flow produced by the syringe pump is steady. Measurement of the velocity profile in the z-direction is completed at the center of the channel where the effects of the channel walls are minimal on the velocity profile. The general procedure is to then set the flow condition and take a sequence of measurements at different heights of the channel. The location of the measurement is represented in Figure 2-10.

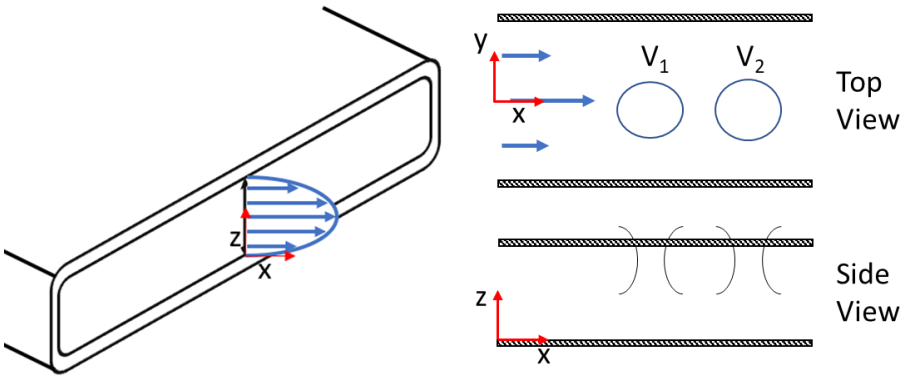

Figure 2-10. *Measurement of the velocity profile taken at the center of the channel and the top and side view of the two beams aligned with the direction of the flow is depicted.*

The data acquired from the APD is the number of photons counted per second in each focal volume which is then cross-correlated between the two volumes to determine the time it takes for the same group of fluorescent molecules or fluorescent particles to pass from one volume to the next. With the time it takes to cross from one volume to the next and the distance known, the velocity in that region can be determined by taking the ratio of the two. The cross-correlation can be completed by the ISS VistaVision software, but output precision is limited since the peak correlation is partitioned into increments of the log scale. Instead, the raw data is extracted from the ISS VistaVision software as a text file and ran through a MATLAB script to complete the cross-correlation between the focal volume, smooth the data, fit the data to a gaussian function and extract the peak correlated time. The velocity can then be determined by taking the ratio of the distance between the focal volume and peak correlated time.

2.2.3.3 Peak Time Extraction

Extraction of peak cross-correlation time can be completed through the ISS VistaVision software which is completed using a multi-tau cross-correlation scheme or through a MATLAB script developed following the methodology of Brinkmeier *et al.* [54]. For this study, the peak cross-correlation time is originally extracted manually from the ISS VistaVision software, however issues of discretization of the time value to whole log values resulting in smaller temporal resolution and therefore velocity resolution. A MATLAB script is written which completes the forward and backward cross-correlation of the fluorescence intensity data, calculate the difference curve, which represents the pure cross-correlation, smooth the data, fit the cross-correlation data with a first order-gaussian fit, and extract the peak time where the maximum value of the fitted cross-correlation function occurs. The peak time data is then exported and stored to an excel data file and the fitted cross-correlation curve is saved for further inspection. A sample cross-correlation curve is represented in Figure 2-11.

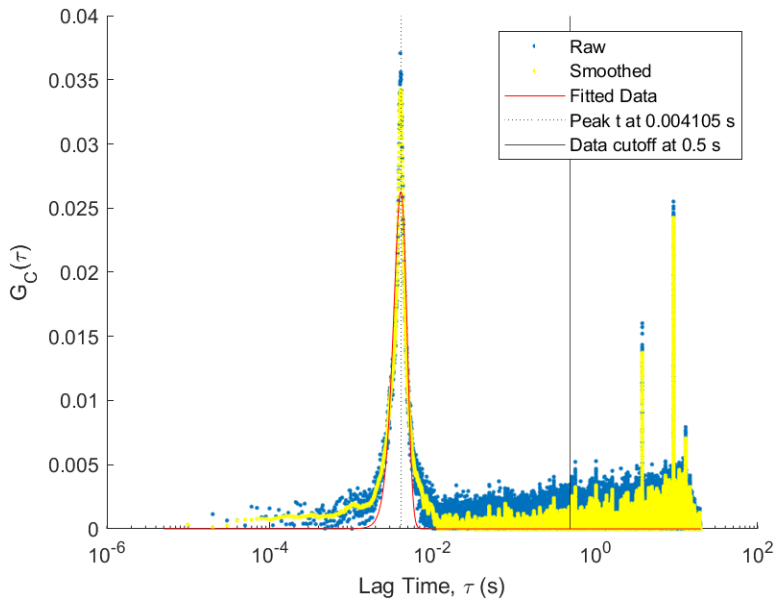

Figure 2-11. *Example cross-correlation curve calculated, smooth and fitted from fluorescence intensity data obtained from the ISS VistaVision software.*

2.2.3.4 System Performance Investigation

For the 2bFCCS experiments, a series of system performance tests are completed to calibrate and identify parameters that would potentially affect the velocity measurement. The series of tests are as follows: fluid admissibility, effect of laser intensity on inducing photobleaching, and velocity measurement performance.

To observe which type of fluid combination is admissible for measuring velocity profile three combinations are tested: when the fluid is diluted with low concentration fluorescent molecules without any additional microparticles, when the fluid is non-fluorescent and is suspending fluorescent microparticles, and when the fluid is diluted with high concentration fluorescent molecules and is suspending non-fluorescent microparticles. The purpose of testing these combinations is to determine alternative fluid configurations that are feasible and used to measure velocity profiles.

To observe the effects of the laser power intensity on photobleaching the diffusion coefficient and counts per second are taken at a range of intensity. Photobleaching is the effect where the fluorescent molecule is permanently altered and is unable to fluoresce. For FCS, photobleaching would artifactually decrease

diffusion time and reduce cross-correlation values during measurement. The laser intensity is tested between the range of 97 µW to 1470 µW.

Lastly, to test the 2bFCCS measurement performance on measuring the velocity profile in a rectangular channel, a series of measurements is made at increments of 10 ticks from the bottom of the channel to the center of the channel at an input flow rate of 5,000 µL/hr. The input fluid used is an Alexa 647 and DI water solution at 1/100,000 dilution. The velocity profile obtained traversing the z-axis is taken at the midpoint and compared to the theoretical velocity profile for an infinitely wide and narrow channel with the pressure gradient defined by the approximated flow rate of a rectangular channel (Equation (3), Section 1.2.4.1) and is represented in Figure 2-12 for a flow rate of 5,000 µl/hr.

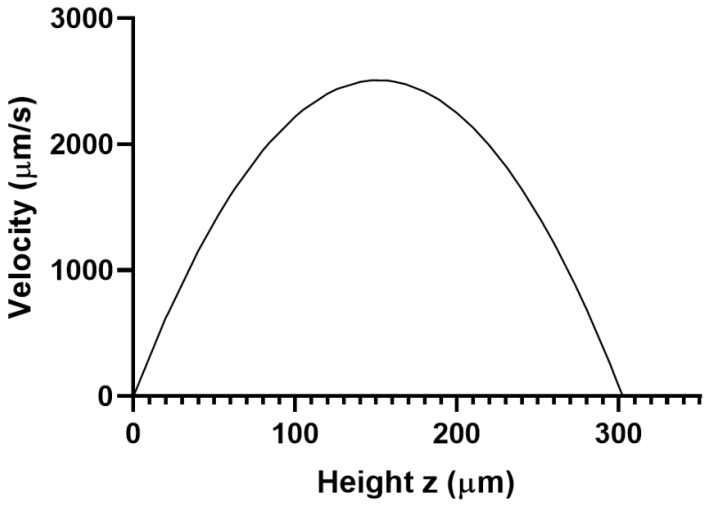

Figure 2-12. *Theoretical velocity profile at 5,000 µl/hr at the center of a 300 µm by 2 mm rectangular channel.*

3 Micro PIV Experiment

This chapter presents the results obtained for the measurement of the velocity profile, rate of shear, CFL thickness and blood layer thickness in the co-flow PDMS device using the µPIV and high-speed camera setup. Furthermore, the results are discussed comparing the experimental measurements to the analytical approximation made and conclusions are made on improvements that need to be addressed.

3.1 Results

3.1.1 Velocity Profile of Blood Layer

The velocity profile is extracted from the blood layer for each flow ratio configuration and input blood flow rate (Section 2.1.3.2). The velocity profiles of the blood layer at each input blood flow rate of 50 µl/hr, 100 µl/hr and 250 µl/hr are organized by flow ratio configuration of 1, 4 and 8 between the PBS and glycerol solution flow rate to the blood flow rate in Figure 3-1. From the µPIV analysis, each testing condition has a flat velocity profile for a significant portion of blood layer thickness. Taking the average velocity across the blood layer a linear relationship between the average velocity and input flow rate is seen for flow ratio 4 and 8, while velocity measurement at 250 µl/hr deviates for the flow ratio of 1. The average velocity for each input blood flow rate is depicted in Figure 3-2.

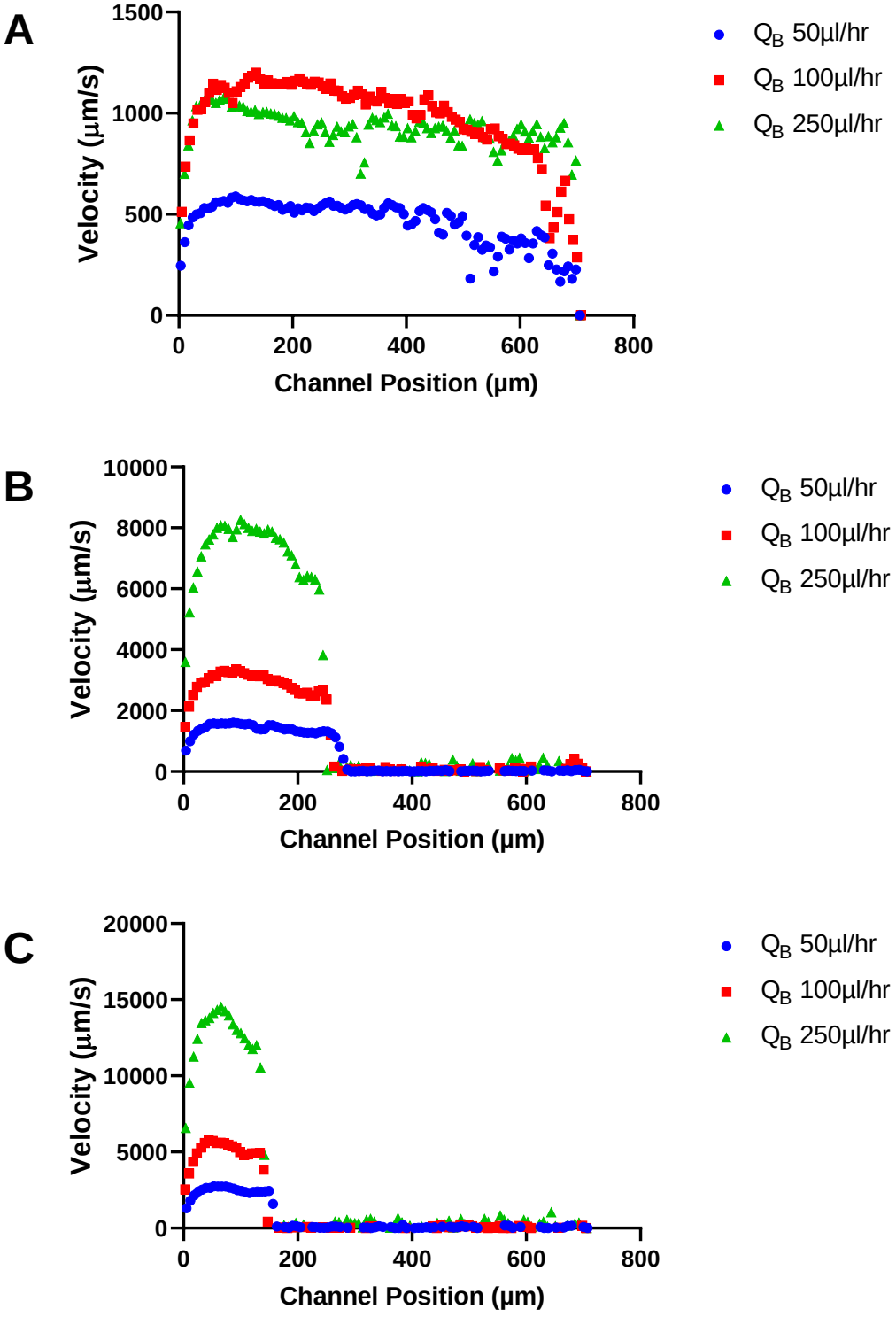

Figure 3-1.*Velocity profile of the blood layer from the µPIV trials of 10% HT blood sample organized by flow ratio configuration of (A) 1, (B) 4 and (C) 8 between the PBS and glycerol solution to blood sample. Each figure displays input blood flow rate of 50 µl/hr, 100 µl/hr and 250 µl/hr.*

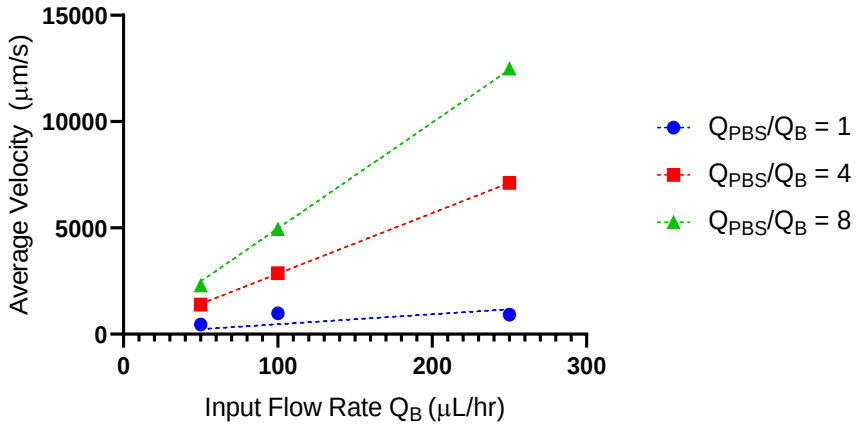

Figure 3-2. *Average velocity profile of the blood layer at each input blood flow rate of 50 µl/hr, 100 µl/hr and 250 µl/hr fitted with linear regression.*

3.1.2 Rate of Shear Across Blood Layer

From the velocity profile of each flow rate and flow ratio configuration, the rate of shear is approximated by fitting a linear velocity profile between the channel wall and fluid interface (Section 2.1.4). Samples for input blood flow rate of 100 µl/hr are depicted in Figure 3-3. Since the analysis of the rate of shear is done by fitting the velocity profile, the same trend is observed where an increase in the input blood flow results in an increase in the measured rate of shear. Due to the flattened velocity profile of the blood layer in the channel and deviation from the expected Couette profile, the rate of shear analysis does not extract a meaningful value of the rate of shear in the blood layer.

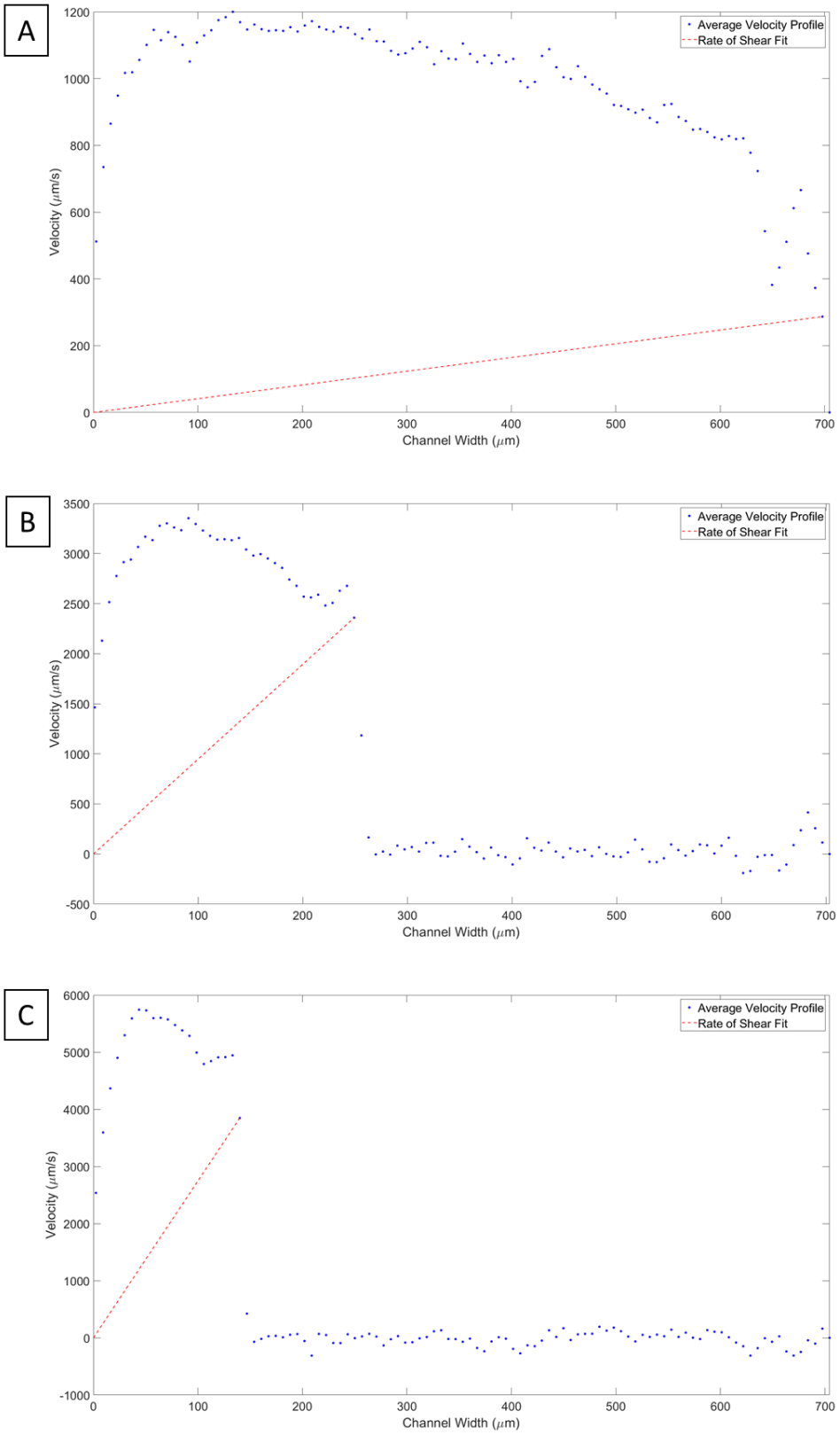

Figure 3-3*. Example of rate of shear analysis for flow ratio configuration of (A) 1, (B) 4, and (C) 8 between the PBS and glycerol solution to blood sample for input blood flow rate of 100 µl/hr.*

3.1.3 Blood Layer Thickness

The thickness of the blood layer is extracted in the process of approximating the rate of shear in the blood layer (Section 2.1.4) and identified during CFL thickness extraction when determining the location of the wall and fluid interface (Section 2.1.5). From the analytical solution, the thickness of the blood layer is expected to be independent of the magnitude of the input blood flow rate. The measurements for each flow configuration are averaged across all input blood flow rate and summarized in Figure 3-4.

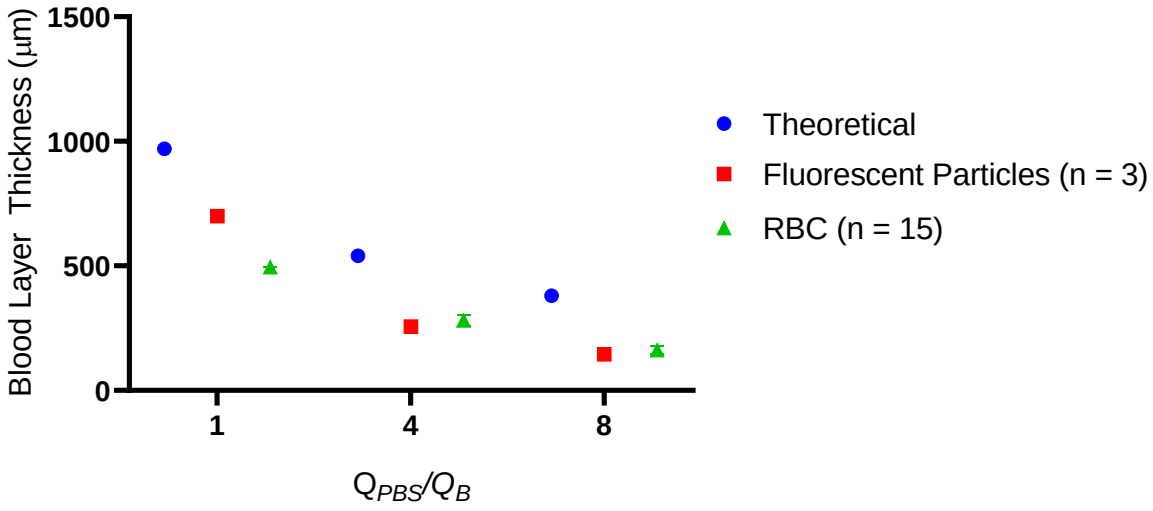

Figure 3-4. *Thickness of Blood layer between theoretical and measured results of each flow ratio configuration from fluorescent particles imaging from the velocity analysis and RBC imaging from the CFL analysis. Error bars indicate ±1 standard deviation for each data set.*

Measurement of the blood layer thickness for a flow ratio configuration of 1 is not valid as the field of view of the imaging did not span the full width of the channel for both the velocity field and CFL analysis. From the fluorescent particle imaging, the average thickness and standard deviation of 256 ± 12 µm and 145 ± 12 µm for flow ratio of 4 and 8, respectively. While for the RBC imaging, the average thickness and standard deviation of 281 ± 23 µm and 162 ± 16 µm for flow ratio of 4 and 8, respectively.

3.1.4 Cell Free Layer Measurement

From the high-speed camera and bright light recording of the RBC the CFL thickness is extracted (Section 2.1.5). The location at 5 positions along the length of the channel for each flow ratio configuration and input blood flow rate is extracted for the CFL providing a spatial averaging across the length of the channel. The measurements are summarized in Figure 3-5.

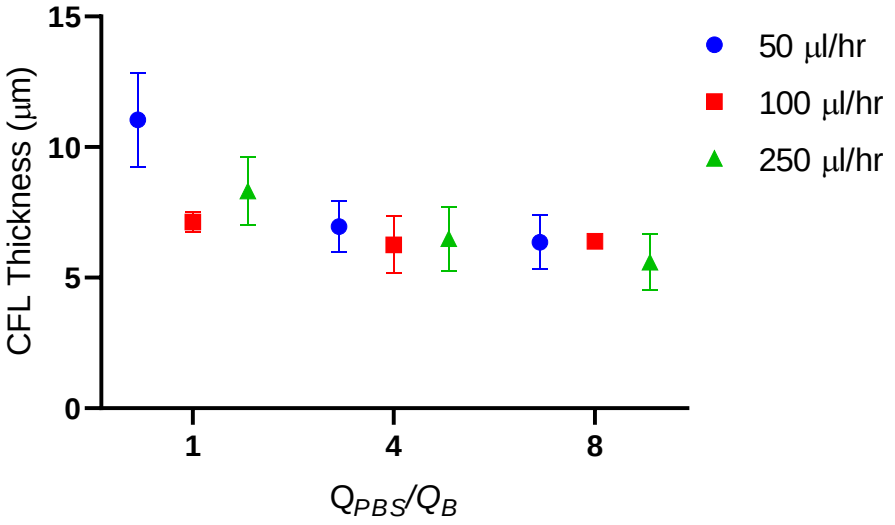

Figure 3-5. *CFL thickness from kymograph taken at 5 locations across the length of the channel for each flow ratio configuration and input blood flow rate. Error bars indicate ±1 standard deviation for each data set composed of the 5 positions.*

3.2 Discussion

3.2.1 Measurement Evaluation

Using the μPIV dual pulsed setup, the velocity profile in the blood layer is extracted successfully. For each flow ratio condition, the results are consistent to each other, where an increase in input blood flow resulted in a linear increase in the magnitude of velocity with the exception for the flow ratio of 1 at an input blood flow rate of 250 μl/hr having similar measurement to the input blood flow rate of 100 μl/hr. From the testing completed by Curtis Armstrong [58], the PDMS chip response time for the same channel design takes less

than 20 seconds to achieve a stable flow rate. The discrepancy of achieving the same velocity magnitude between the 100 µl/hr and 250 µl/hr trial may be due to insufficient time for the syringe pump to stabilize the testing flow rate which would result in a reduction in measured velocity. However, with the current methodology the syringe pump is controlled externally using a command terminal setup and is programmed between each test case. Furthermore, since each test case only contains a single trial the more probable cause is due to human error with controlling the syringe pump from the computer command prompt to have the proper inputs before taking the PIV data. Future protocol in utilizing the external control should explore more vigorous verification methods of the velocity profile.

From the sample velocity measurement of the blood layer, Figure 3-1, we can see that the experimental results deviate from the idealized linear velocity profile expected in the blood layer from using the co-flow device. A significant portion of the velocity profile is plateaued between the channel wall and the fluid interface which means the velocity gradient and therefore the local rate of shear in this region is zero. Furthermore, this would indicate that the current flow ratio configuration and input blood flow rate is suboptimal for the current channel geometry in having a controlled rate of shear applied to the blood sample. In comparison, Curtis Armstrong [58] was able to achieve a linear velocity profile by utilizing a higher flow ratio of 25, and Rym Mehri [61] achieved a linear velocity in the blood layer utilizing a channel with a 110 µm by 60 µm rectangular cross-sectional area. For a controlled comparison analysis relating the rate of shear applied to the blood sample and the formation of the CFL thickness, a larger flow ratio should be explored where the blood layer is narrower, and the velocity profile is more linear.

Completing the procedure to extract the rate of shear it is clear that a linear fit does not appropriately represent the velocity gradient in the blood layer as seen in the example conditions in Figure 3-3. The linear fit both underestimates the local rate of shear experienced in the region closest to the wall and overestimates the rate of shear in the region where the velocity has plateaued. Therefore, compared to the study by Rym Mehri [61], using the a linear fit does not model the rate of shear with the current channel design and flow configuration. Furthermore, there is a large discrepancy in the magnitude of the rate of shear between the

theoretical mean rate of shear obtained from the analytical model and the experimentally measured rate of shear from the μPIV analysis. A larger measured rate of shear would indicate that either the velocity at the fluid interface is greater than predicted or the width of the blood layer is less than predicted.

From the fluorescent particle and RBC imaging, the blood layer thickness is experimentally determined in the co-flow device and is found to be significantly less than the theoretical prediction. Between the fluorescent particle and RBC imaging, no statistical difference was observed at the flow ratio of 4 and 8, while the flow ratio of 1 had limitations on the field of view of the optical setup. This provides confirmation on the feasibility of using fluorescent particles to determine the width of the blood layer for the rate of shear analysis. However, further investigation should be made to verify reliability utilizing higher magnification to improve spatial resolution. Although the fluorescent particles and RBC imaging produced similar results, both techniques found that the experimental measurement of the blood thickness is lower than the theoretical prediction for all flow conditions.

The discrepancies between the theoretical and measured thickness could be due to the co-flow still being in a transient state after the fluids converges since the channel cross-sectional width (2,000 μm) of the channel is not significantly smaller than the length (9,000 μm) of the converged channel. However, further investigation is required to confirm if the channel length is insufficient to produce a fully developed velocity profile. In which case a narrow channel with a longer length should be utilized.

Lastly, the CFL thickness is extracted from the kymograph using the high-speed camera and bright light setup. Using a kymograph has the advantage to be applicable to any channel geometries, giving the local CFL regardless the curvature of the channel (if any) which will induce CFL heterogeneity. The original methodology was to compare the CFL with a constant rate of shear, however with the measurements the rate of shear applied to the blood layer with the current flow configuration selected clearly is not constant. To improve the CFL analysis, a greater magnification should be evaluated to increase the spatial resolution and separation between the condition. With the current magnification, a large portion of the field of view is not fully utilized and is not adding additional information.

3.2.2 Analytical Solution Shortcoming

The analytical solution used to complete the planification of the testing condition of the blood sample assumes that the co-flow is two incompressible immiscible Newtonian fluids that have fully developed velocity profile and are unidirectional through infinite plates. From the measurements, the results obtained did not meet expectations on determining the magnitude of the rate of shear and the thickness of the blood layer for the selected microfluidic channel design.

The assumption that the fluid is Newtonian is incorrect and does not account for the non-Newtonian nature of blood in microflow, however the implementation for a Newtonian fluid is simpler and for the planification stage should have been enough at identifying the general magnitude of the velocity profile and rate of shear. The assumption that the fluid is a 2-d uniflow through infinite plate resulted in a significant underestimate of the velocity magnitude since it assumes that there is an equal distribution of the flow rate along the height of the channel. However, in the physical application the wall effects of the top and bottom wall are significant and a large velocity at the midplane of the channel should be expected for the input flow rate. Lastly, the assumption that the fluid is fully developed and steady needs to be verified to ensure that profile and blood layer thickness is not changing along the length of channel. Future work of verifying the channel design and analytical solution can use water with fluorescent particles to identify the velocity profile within the channel.

3.3 Conclusions

Using the µPIV setup and high-speed camera setup it was possible to extract the velocity profile, blood layer thickness and CFL thickness. With the current flow ratio configuration and input blood flow rate, the velocity profile deviates from the linear profile required to achieve a controlled rate of shear in the blood layer. With the current flow rate configuration and input flow rate the thickness of the blood layer and velocity magnitude was found to be much less than the predicted model resulting in a rate of shears that are significantly greater than predicted. Comparing the 2-D analytical model to the experimental results

highlights the limitations of the assumptions made for the model. The assumption that the flow was a 2-D infinite plate for a narrow rectangular channel underestimated the experimental velocity magnitude and rate of shear. While the Newtonian assumption did not account for non-Newtonian nature of the blood layer. Furthermore, investigation of the entrance length of the selected microfluidic device needs to be verified to ensure that the assumption the flow was fully developed was valid. To improve the measurement of the velocity profile, larger flow ratio should be explored to verify if a thinner blood region can produce the desired linear profile. While to improve spatial resolution of the fluorescent particle and RBC recording, a larger objective magnification should be utilized to obtain a closer imaging of the blood layer and the CFL, and fully utilizing the field of view of the recording.

4 Two-beam FCCS

This chapter outlines the results obtained for the system performance investigation of the 2bFCCS system at the Centre de Biologie Structurale (CBS) in Montpellier observing the fluid admissibility, photobleaching validation and velocity measurement. The results are discussed, and conclusions are made on future work required.

4.1 Results

4.1.1 Fluid Admissibility

Different fluids with variation of fluorescent molecules, fluorescent and non-fluorescent particles are tested to verify which combination can be selected to achieve a clear correlation to extract the peak lag time. The combinations that are explored are a standard solution of fluorescent molecule diluted at 1/100,000 in DI water, a suspension of fluorescent particles diluted at 1/100,000 in DI water, a suspension with non-fluorescent particles diluted at 1/10 the concentration in of a solution of fluorescent molecule diluted at 1/1,000 in DI water and lastly a blood sample set at 40% HT with fluorescent molecule diluted at 1/1,000. For each fluid combination, fluorescent intensity measurements are made within the glass capillary rectangular channel and sample correlation is extracted using inhouse MATLAB script (Section 2.2.3.3). Intensity measurements are presented in Figure 4-1 for a height of 63 μm from the bottom of the channel.

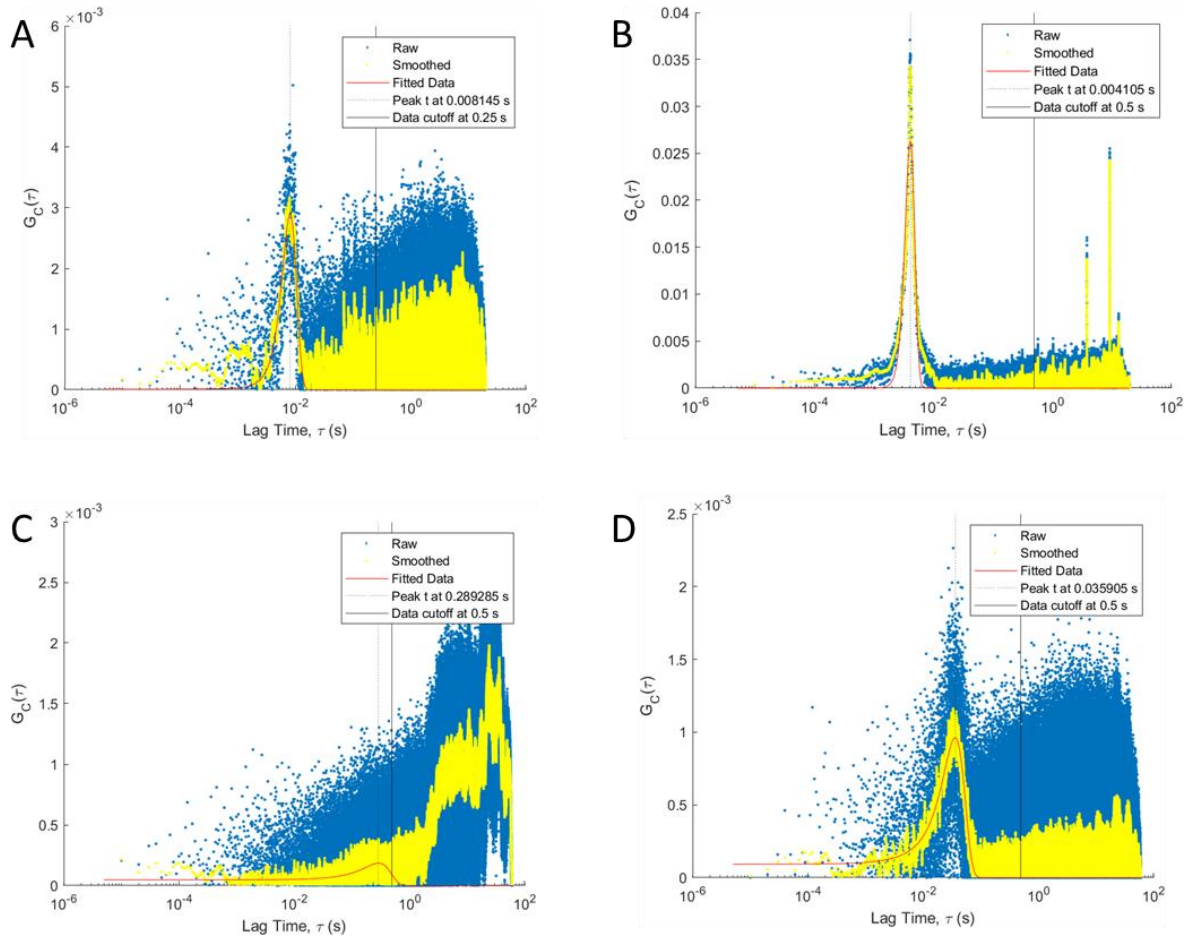

Figure 4-1. *Sample correlation results for (A) standard solution with Alexa 647 at x100,000 dilution, (B) dark red fluorescent particles at x100,000 dilution, (C) non-fluorescent bead at x10 dilution with Alexa 647 at x1,000 dilution, (D) 40% HT blood sample with Alexa 647 at x1,000 dilution. Flow rate is not controlled between sample fluid.*

4.1.2 Laser Induced Photobleaching

To test the effect of the laser intensity on photobleaching the fluorescent molecule, diffusion time and photon counts per second for a range of laser intensity is presented in Figure 4-2 and Figure 4-3. From the results, we see that with increasing laser intensity there is an increase in the photon counts per second and a reduction in the diffusion time.

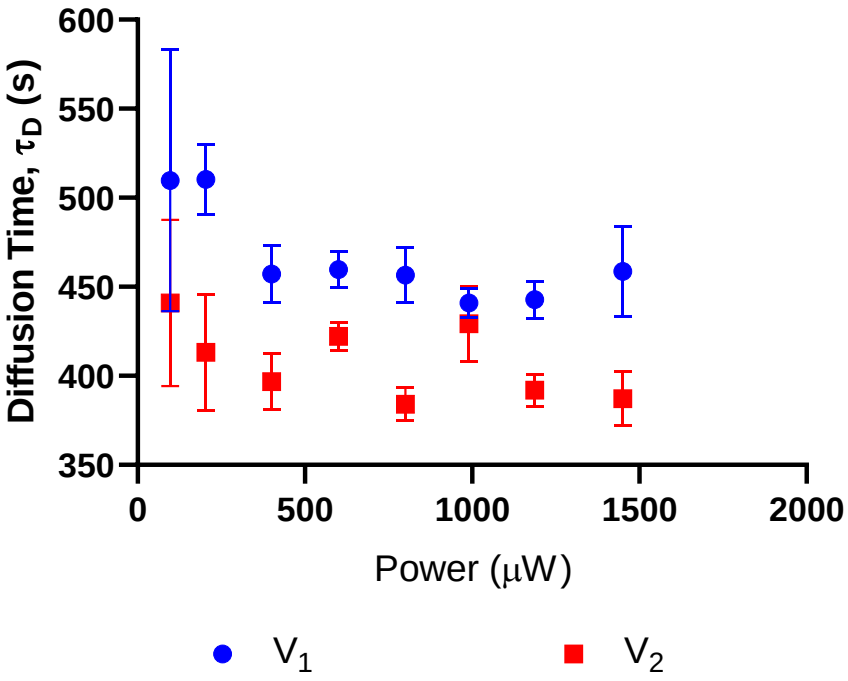

Figure 4-2. *Effect of power intensity on diffusion time in each focal volume.*

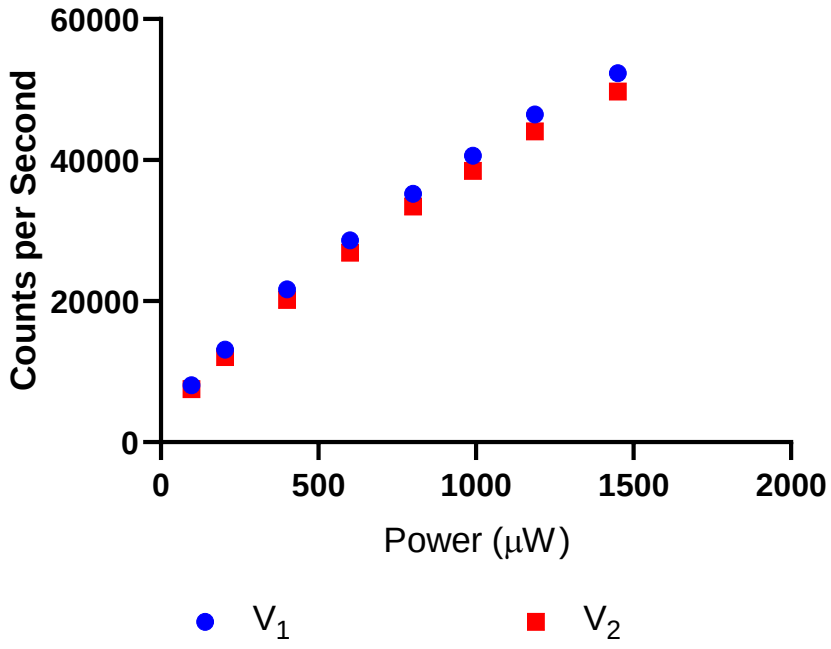

Figure 4-3. *Effect of power intensity on photon counts in each focal volume.*

4.1.3 Velocity Measurement in Rectangular Capillary

The 2bFCCS system was not tested prior to arriving in the lab and one of the main objectives is to identify if the system is able to determine the velocity in a microfluidic device. The velocity profile in the channel is determined by manually taking measurements along the height following the methodology outlined in Section 2.2.3. The results of the velocity profile measurement in the channel at 5,000 µl/hr and 10,000 µl/hr with the theoretical velocity profile are presented in Figure 4-4 and Figure 4-5, respectively.

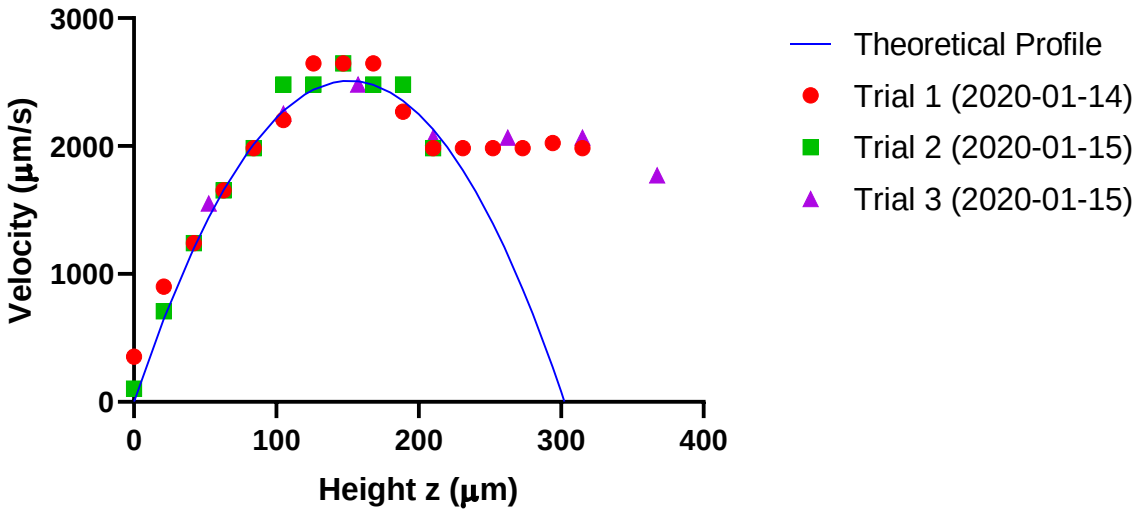

Figure 4-4. *Velocity profile in 302.4 µm by 2,000 µm rectangular glass capillary channel with Alexa 647 diluted to 1/100,000 the original solution in DI water flowing at 5,000 µl/hr.*

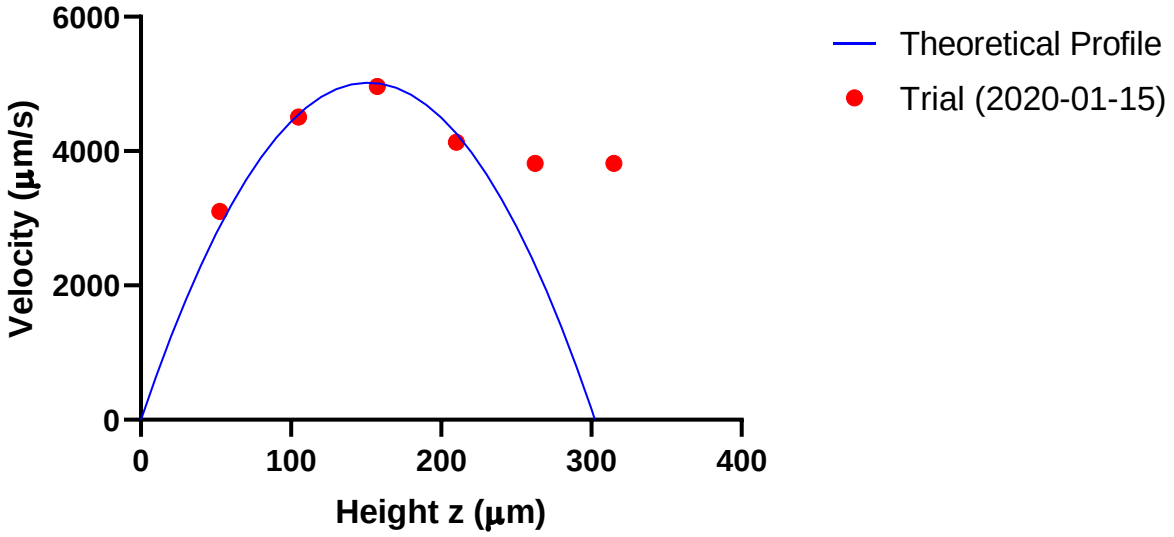

Figure 4-5. *Velocity profile in 302.4 µm by 2,000 µm rectangular glass capillary channel with Alexa 647 diluted to 1/100,000 the original solution in DI water flowing at 10,000 µl/hr.*

The range of velocity that the 2bFCCS can measure is also tested under various power levels and the result is presented in Figure 4-6.

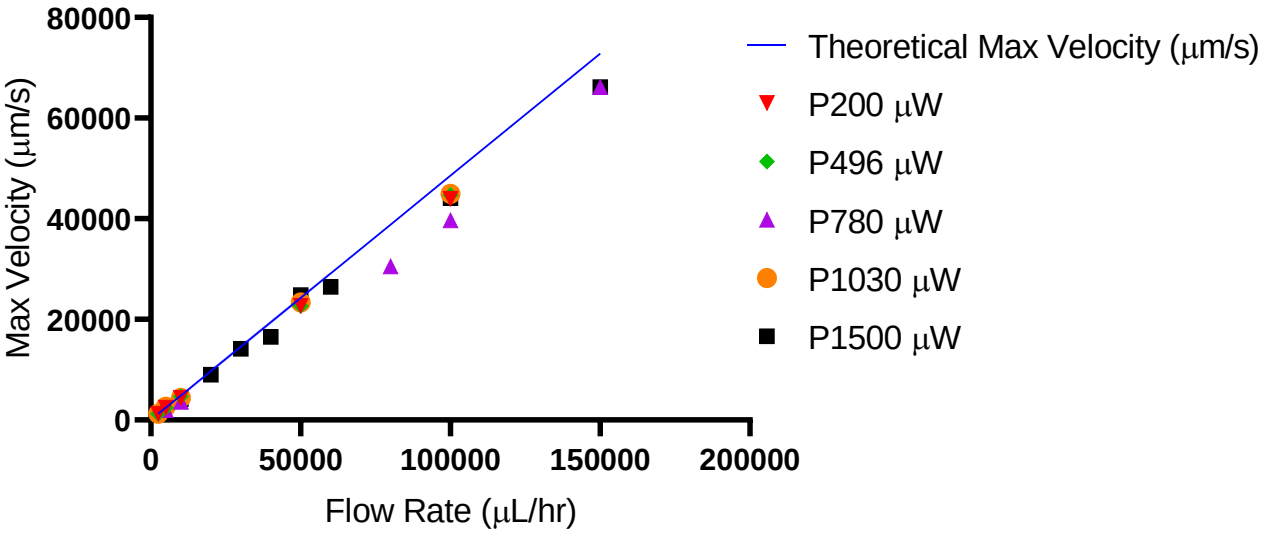

Figure 4-6. *Peak velocity measurement taken at the center of the channel under various power levels.*

Lastly, measurement of the velocity profile of 40% blood with high concentration Alexa 647 flowing through the rectangular channel is presented in Figure 4-7.

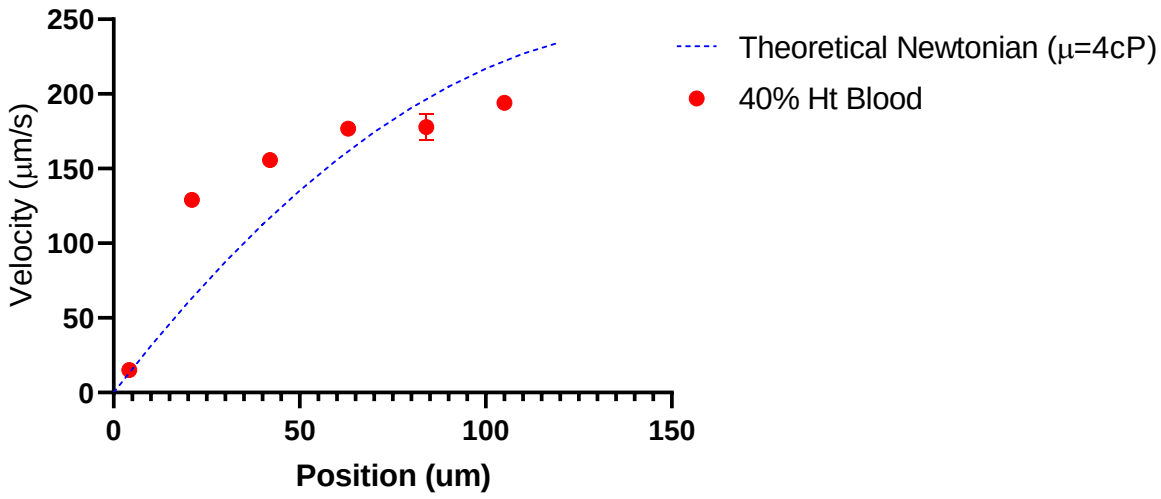

Figure 4-7. *Velocity profile of 40% HT blood sample with Alexa 647 diluted to 1/1,000 concentration in the 302.4 µm by 2,000 µm rectangular glass capillary channel.*

4.2 Discussion

4.2.1 Fluid Admissibility

As part of the testing of the 2bFCCS, we looked at the different fluorescent components that can be used to extract the velocity profile within a microfluidic device. From theoretical derivation of the correlation function, it is known that the magnitude of the correlation function is inversely proportional to the number of fluorescent molecules [54]. The standard solution of low concentration fluorescent molecules and the solution of low concentration fluorescent particles were expected to work since both utilized a low concentration of molecules. The difference between the two samples is that the fluorescent molecule is homogeneously distributed throughout the solution in contrast to being densely packed in individual particles suspended in the fluid. Between the two conditions, the fluorescent beads fluorescent fluctuation data has very large distinct peaks when the particles pass through the focal volumes. This limits the

maximum laser intensity when using fluorescent particles as the APD has a saturation limit on how much light it can receive. For measuring the velocity profile, both fluorescent molecules and fluorescent particles can be used to obtain peak lag time for the velocity as seen in Figure 4-1 (A) and (B).

The third sample condition, high concentration fluorescent molecule with opaque non-fluorescent beads, is to test if it is possible to extract peak lag time from fluorescent fluctuations induced when non-fluorescent beads displace the dense fluorescent molecules in the focal volume. The concept of an inverted FCS has been accomplished previously by Wennmalm *et al.* [56]. However, with the current setup used in the lab, the fluorescence fluctuation data produced correlations that are relatively noisier and peaks less significant making extraction of peak lag time more difficult as seen in Figure 4-1 (C). The fiber aperture is significantly larger than the pinholes in comparison to the original study by Wennmalm *et al.* [56] and therefore the size of the focal volume is also significantly larger. With a large focal volume, the quantity and size of the non-fluorescent beads may not significantly displace the fluorescent molecules to induce fluorescent fluctuation.

The last tested sample condition is blood with a high concentration fluorescent molecule diluted in the suspending fluid. Initially, blood samples of 1%, 5%, 10% and 40% HT were tested. The most promising results are obtained from the 10% and 40% HT samples, in producing distinguishable peaks in the correlation curve. A sample correlation of the 40% HT is presented in Figure 4-1 (D). The third condition with non-fluorescent beads, where non-fluorescent particles are blocking the fluorescent molecules to induce fluorescent fluctuations in the focal volume, was chosen as an analogous of blood sample. However, differences in the size, geometry and opacity of the non-fluorescent particle may play a role in the efficacy of the fluid. Since RBC are highly deformable, and significantly larger than the fluorescent beads they may be more ideal at displacing the fluorescent molecules in the focal volume.

The results obtained from testing high HT blood samples are promising because high-density samples are typically difficult to measure for other optical measurement techniques like µPIV. Indeed, the increase in cell concentration reduces the lighting of the sample in bright light and reduces visibility of the fluorescent

particles when using the dual pulsed laser. With a higher density suspension, fluorescent particles become less visible as the suspended cells are blocking the tracer particles which generally results in an increase of spurious velocity measurements.

4.2.2 Laser Induced Photobleaching

Photobleaching is when fluorescent molecules are altered such that they are unable to fluoresce when excited. For FCS, photobleaching induced by a high-intensity laser would artifactually reduce the measurement of the diffusion time and cross-correlation value during measurement. To test whether the laser intensity had a significant effect on the fluorescent molecules, diffusion time and photon counts per second, which are derived parameters of the fluorescence fluctuation data, is measured within the working range of laser intensity as seen in Figure 4-2 and Figure 4-3. For this application, the working range 0 to 1500 µW is selected respecting the FCS system safety limit on the maximum possible light measured by the APD to protect the sensors from being damaged from high intensity light. Within the working laser intensity, the effect of photobleaching by the laser is found to not be a significant issue since only a slight decrease in diffusion time is observed and the photon counts are still increasing within the range of laser intensity. For photobleaching to be considered significant, the counts per second is expected to reach a plateau while the diffusion coefficient would trend to zero.

4.2.3 Velocity Measurements

From the velocity trial in Figure 4-4 and Figure 4-5, it is observed that the velocity profile shape follows closely to the theoretical approximated velocity profile for a rectangular channel. The experimental data points are dispersed unevenly across the z-axis since the physical movement of the platform is completed manually using the microscope fine adjustment. With repeated measurements, there is some variation in the magnitude of velocity in between trials and relative to the theoretical velocity profile, which can be caused by the angle of the beam, and precision of the microscope steps.

The position of the two focal volumes is manually aligned to be parallel to the flow. However, since this is completed manually there is an inherent error to the precision of the alignment. If the two focal volumes are not aligned to the direction of the flow, the velocity measured is a projection of the maximum velocity into the direction between the two focal points. To account for the deviation of the focal volume angle to the flow direction, images of the two beams and the channel wall can be taken for post-processing correction. Like the angle of the beam relative to the direction of the flow, the positioning of the beam in the z-direction is also controlled manually with the microscope fine adjustment. During testing, this control is completed in a dark room where visibility of the ticks is limited, and this is to prevent over saturating the APD with the room's light. Misalignment of the fine adjustment ticks can result in additional imprecision. To address both issues, the use of motorized microscope stages with piezoelectric sensors to detect displacement can improve on the manual control of positioning the focal volume in the channel.

Furthermore, from Figure 4-4 and Figure 4-5, the velocity measurement made after 200 μm appear to plateaued. However, since the channel is symmetrical the velocity profile should also be symmetrical along the mid-plate. The plateau is due to the limitation of the objective lens selected for the experiment. With the x63 objective lens, the max free distance that can be observed is 0.28 mm with a 0.17 mm cover glass. For the glass capillary microfluidic device, the thickness of the capillary walls is approximately 0.210 mm ± 10% tolerance. Therefore, the maximum free distance is approximately 0.24 mm and it is not possible to traverse the whole width of the channel. For future tests, a smaller channel or a glass capillary with thinner walls can be used.

At the channel wall there is the no-slip condition and as a result the expected velocity at the wall should be zero. However, with the 2bFCCS measurement, there is a measurable velocity at the surface of the wall which is most likely due to the geometry and spatial limitation of the focal volume made by the confocal microscope. With the confocal microscope, the focal volume is an elongated oval aligned in the z-axis and circular in the x-y plane. When focusing the two focal volumes at the wall, which is identified by having the two laser points to be the smallest through the eyepiece, a portion of the focal volume is always inside

of the channel as the center of the volume is set at the wall. The result is that emitted light from the fluorescent molecule will always be non-zero when taking measurements at the wall and therefore the velocity will also be non-zero.

The secondary velocity measurement test is to observe the range of velocity that the 2bFCCS can measure. Using a range of power and the standard solution of Alexa 647, input flow rate between 2,500 µl/hr to 150,000 µl/hr is measured in the rectangular channel obtaining velocity between approximately 1,200 µm/s to 70,000 µm/s as seen in Figure 4-6. At higher flow rates after 50,000 µl/hr, the velocity measurements appear to deviate away from the theoretical maximum velocity. This may be due to misalignment of the beam after refilling the syringe inducing a slower velocity measurement or it may be an indication of instability of velocity measurements at higher flow rates. However, further investigations would be required to understand the cause of deviation between the theoretical velocity and measured velocity at higher flow rate. The range of velocity measurements obtained follows results from studies using similar 2bFCCS setups [52, 54]. The advantage of having a range of velocity between 10 µm/s to 10 cm/s is invaluable for testing a great range of flow conditions without changing the optical setup between tests as it should be done in µPIV.

Lastly, a testing on identifying the velocity profile of 40% HT blood sample with high concentration of Alexa 647 is presented in Figure 4-7. The result of flowing the blood sample produced a plug velocity profile in comparison to the parabolic velocity profile of a Newtonian fluid with a similar bulk viscosity of 40% HT blood. The plug velocity profile of the blood sample is characteristic of a shear thinning fluid. The result of the testing is promising as measurement of high HT blood samples are typically very difficult to accomplish using other optical techniques like µPIV as the cell concentration typically blocks too many of the fluorescent particles required to achieve a good velocity field measurement.

4.3 Conclusion

Within the time frame available during the visit to the lab in CBS, the 2bFCCS system was tested for fluid admissibility, laser-induced photobleaching and a variety of velocity performance measurements. Different fluid combinations were tested, and it was found that the non-fluorescent beads with high concentration fluorescent molecules produced the least distinguishable correlation curves. However, the high concentration blood sample with high concentration fluorescent molecules in the suspending fluid is found to show promising results in obtaining distinguishable peak lag time. The 2bFCCS system was also found to not have significant photobleaching effects within the range of 0 µW to 1500 µW of the laser intensity range with the fluorescent sample concentration. In the velocity measurement performance verification, it was found that the 2bFCCS can measure the velocity profile of the rectangular channel that conforms with the theoretical velocity profile. However, for future tests, the size of the channel should be considered if complete velocity profile measurements are required. Furthermore, it was found that the range of 10 µm/s to 10 cm/s of velocity is measurable with the system without changing the optics. Lastly, from measurements profiling the channel with blood samples, it was found that high concentration blood produced a plug flow which is expected of a shear-thinning fluid. From this verification study, 2bFCCS is a promising measurement tool for the use of characterizing blood microflow.

5 Proposal for Future Work

The field of blood rheology is not limited to the biological function of blood flowing through the circulatory system. It has impacts on many biomedical applications where precise blood flow handling is necessary such as dialysis, blood transfusion or even the design of next-generation microfluidic diagnostic tools [62].

Understanding blood rheology however is still in its infancy. Where research in hemorheology in the 20th century, has either been descriptive when focusing on microcirculation, such as revealing local RBC HT being heterogeneous [2], or classical, such as showing blood apparent viscosity decreasing with an increase forces of the flow [1, 3]. Despite these pioneering discoveries, the lack of new approaches of deciphering the role of blood structure on its bulk flow and in the microcirculatory conditions keeps the study of blood rheology in its potentialities. In fact, classical rheological measurement of viscosity has no real meaning for the case of complex fluids. The viscosity of a fluid is extracted from the torque measurement in rheometers while considering a homogenous ideal linear velocity profile in the bulk fluid, as seen in Figure 1-3.

In collaboration between the University of Ottawa and University de Montpellier, the long-term goal is to couple the bulk rheological measurement of blood flow with the characterization of local microstructures phenomena when blood flows through both simple and complex geometry. Thereby bringing a true description of blood rheology. The collaboration has been developing new tools to tackle this problem over the past three years and this project will be continued in a PhD to focus on utilizing these available tools to study blood rheology and the experimental results required to provide the first elements of a blood constitutive law.

At the University of Ottawa, two methods of local measurement of rheology can be employed. The first is the use of a pressure-flow viscosimeter method, where a custom-made platform combines an optically clear PDMS channel with integrated pressure measurements. This method allows for the direct measurement of the change in pressure and flow rate, allowing for bulk viscosity measurements across the channel. It will

be paired with local microstructure observation using a high-speed camera setup, and local shear characterization using μPIV. The second method is the use of the co-flow PDMS channel design as presented in this thesis to evaluate the apparent viscosity of the blood suspension in microchannels which utilizes the concept of optical viscometers [32]. The analytical solution of two co-flowing laminar streams in a rectangular channel can be utilized to obtain the viscosity ratio as a function of the flow rate ratio. Similarly, the velocity field and microstructure can be observed using the μPIV and high-speed camera setup.

At the University de Montpellier, the 2bFCCS system will be coupled with a state-of-the-art rheometer. Measurement of the structure of blood flow will be evaluated by determining the spatial distribution in volume fraction and the velocity field within the bulk of the rheometer using the 2bFCCS system while simultaneously measuring the bulk rheometric properties of blood. The velocity measurement capabilities presented in this thesis demonstrates the characterization of the flow field in the rheometer.

The local measurement of blood rheology on the platform developed at the University of Ottawa and the bulk measurement of rheology on the platform developed at the University de Montpellier, are the first step towards the development of a constitutive law for blood.

6 References

[1] T. W. Secomb, “Blood Flow in the Microcirculation,” *Annu. Rev. Fluid Mech*, vol. 49, pp. 443–61, 2017.

[2] E. Kaliviotis, J. M. Sherwood, and S. Balabani, “Partitioning of red blood cell aggregates in bifurcating microscale flows,” *Sci. Rep.*, 2017.

[3] S. Chien, “Shear dependence of effective cell volume as a determinant of blood viscosity,” *Science (80-.).*, 1970.

[4] A. S. Popel and P. C. Johnson, “Microcirculation and hemorheology,” *Annual Review of Fluid Mechanics*. 2005.

[5] R. Fåhræus and T. Lindqvist, “The Viscosity of the Blood in Narrow Capillary Tubes,” *Am. J. Physiol. Content*, 1931.

[6] K. B. Chandran, S. E. Rittgers, and A. P. Yoganathan, *Biofluid mechanics: The human circulation, second edition*. 2012.

[7] E. Ch Mokken, M. Kedaria, C. P. Henny, M. Hardeman, and A. Gelb, “The clinical importance of erythrocyte deformability, a hemorrheological parameter,” Springer-Verlag, 1992.

[8] D. E. Discher, N. Mohandas, and E. A. Evans, “Molecular maps of red cell deformation: Hidden elasticity and in situ connectivity,” *Science (80-.).*, 1994.

[9] R. M. Hochmuth, E. A. Evans, H. C. Wiles, and J. T. McCown, “Mechanical measurement of red cell membrane thickness,” *Science (80-.).*, 1983.

[10] L. Waite and J. Fine, *Applied Biofluid Mechanics*. 2007.

[11] G. Schramm, “A Practical Approach to Rheology and Rheometry,” *Rheology*, 1994.

[12] P. Galambos and F. Forster, “Optical micro-fluidic viscometer,” in *American Society of Mechanical Engineers, Dynamic Systems and Control Division (Publication) DSC*, 1998.

[13] P. Vennemann, R. Lindken, and J. Westerweel, “In vivo whole-field blood velocity measurement techniques,” *Exp. Fluids*, 2007.

[14] R. L. Whitmore, *Rheology of the circulation*, 1st ed. Oxford, New York: Pergamon Press, 1968.

[15] H. L. Goldsmith, G. R. Cokelet, and P. Gaehtgens, “Robin Fahraeus: Evolution of his concepts in cardiovascular physiology,” *Am. J. Physiol. - Hear. Circ. Physiol.*, vol. 257, no. 3 (26/3), 1989.

[16] W. Reinke, P. Gaehtgens, and P. C. Johnson, “Blood viscosity in small tubes: Effect of shear rate, aggregation, and sedimentation,” *Am. J. Physiol. - Hear. Circ. Physiol.*, 1987.

[17] S. Chien and K. ming Jan, “Ultrastructural basis of the mechanism of rouleaux formation,” *Microvasc. Res.*, 1973.

[18] J. J. Bishop, A. S. Popel, M. Intaglietta, and P. C. Johnson, “Rheological effects of red blood cell aggregation in the venous network: A review of recent studies,” *Biorheology*. 2001.

[19] J. K. Armstrong, H. J. Meiselman, and T. C. Fisher, “Evidence against macromolecular ‘bridging’ as the mechanism of red blood cell aggregation induced by nonionic polymers,” in *Biorheology*, 1999.

[20] H. J. Meiselman, “Red blood cell role in rbc aggregation: 1963-1993 and beyond,” *Clin. Hemorheol. Microcirc.*, 1993.

[21] J. Zhang *et al.*, “Fundamentals and applications of inertial microfluidics: A review,” *Lab on a Chip*, vol. 16, no. 1. Royal Society of Chemistry, pp. 10–34, 2016.

[22] H. L. Goldsmith, “Red cell motions and wall interactions in tube flow.,” *Fed. Proc.*, 1971.

[23] G. Coupier, B. Kaoui, T. Podgorski, and C. Misbah, “Noninertial lateral migration of vesicles in bounded Poiseuille flow,” *Phys. Fluids*, 2008.

[24] S. K. Doddi and P. Bagchi, “Three-dimensional computational modeling of multiple deformable cells flowing in microvessels,” *Phys. Rev. E - Stat. Nonlinear, Soft Matter Phys.*, 2009.

[25] B. Kaoui, G. H. Ristow, I. Cantat, C. Misbah, and W. Zimmermann, “Lateral migration of a two-dimensional vesicle in unbounded Poiseuille flow,” *Phys. Rev. E - Stat. Nonlinear, Soft Matter Phys.*, 2008.

[26] T. Secomb, “Mechanics of red blood cells and blood flow in narrow tubes,” 2003.

[27] D. Leighton and A. Acrivos, “The Shear-Induced Migration of Particles in Concentrated Suspensions,” *J. Fluid Mech.*, 1987.

[28] D. S. Hariprasad and T. W. Secomb, “Two-dimensional simulation of red blood cell motion near a wall under a lateral force,” *Phys. Rev. E - Stat. Nonlinear, Soft Matter Phys.*, 2014.

[29] S. E. CHARM and G. S. KURLAND, “Blood Flow and Microcirculation,” 1974.

[30] A. D. Anastasiou, A. S. Spyrogianni, and S. V Paras, “Experimental study of pulsatile blood flow in micro channels,” 2010.

[31] B. E. Rapp, *Microfluidics: Modeling, mechanics and mathematics*. Elsevier Inc., 2017.

[32] R. Mehri, C. Mavriplis, and M. Fenech, “Red blood cell aggregates and their effect on non-Newtonian blood viscosity at low hematocrit in a two-fluid low shear rate microfluidic system,” *PLoS One*, 2018.

[33] R. Mehri, “Micro PIV and Numerical Investigation of a Micro-Couette Blood Flow,” 2013. [Online]. Available: https://ruor.uottawa.ca/handle/10393/22916. [Accessed: 23-Aug-2020].

[34] M. Raffel, C. E. Willert, F. Scarano, and C. J. Kähler, *Particle Image Velocimetry*, 3rd Ed. Springer-Verlag, 2018.

[35] S. T. Wereley and C. D. Meinhart, “Recent Advances in Micro-Particle Image Velocimetry,” *Annu. Rev. Fluid Mech.*, 2009.

[36] B. Wieneke, “PIV Uncertainty Quantification and Beyond,” 2017.

[37] S. J. Williams, C. Park, and S. T. Wereley, “Advances and applications on microfluidic velocimetry techniques,” *Microfluidics and Nanofluidics*. 2010.

[38] M. G. Olsen and C. J. Bourdon, “Out-of-Plane Motion Effects in Microscopic Particle Image

Velocimetry," *J. Fluids Eng. Trans. ASME*, 2003.

[39] S. T. Wereley, L. Gui, and C. D. Meinhart, "Advanced algorithms for microscale particle image velocimetry," *AIAA J.*, 2002.

[40] C. V. Nguyen, A. Fouras, and J. Carberry, "Improvement of measurement accuracy in micro PIV by image overlapping," *Exp. Fluids*, 2010.

[41] K. L. Pitts, R. Mehri, C. Mavriplis, and M. Fenech, "Micro-particle image velocimetry measurement of blood flow: Validation and analysis of data pre-processing and processing methods," *Meas. Sci. Technol.*, 2012.

[42] Y. Sugii, S. Nishio, and K. Okamoto, "In vivo PIV measurement of red blood cell velocity field in microvessels considering mesentery motion," *Physiol. Meas.*, 2002.

[43] L. Bitsch, L. H. Olesen, C. H. Westergaard, H. Bruus, H. Klank, and J. P. Kutter, "Micro PIV on blood flow in a microchannel," *Proc. 7th Int. Conf. Miniaturized Chem. Biochem. Anal. Syst. Oct. 5-9, California, USA*, 2003.

[44] P. Vennemann *et al.*, "In vivo micro particle image velocimetry measurements of blood-plasma in the embryonic avian heart," *J. Biomech.*, 2006.

[45] R. Lima, S. Wada, M. Takeda, K. ichi Tsubota, and T. Yamaguchi, "In vitro confocal micro-PIV measurements of blood flow in a square microchannel: The effect of the haematocrit on instantaneous velocity profiles," *J. Biomech.*, 2007.

[46] R. Lima *et al.*, "In vitro blood flow in a rectangular PDMS microchannel: Experimental observations using a confocal micro-PIV system," *Biomed. Microdevices*, 2008.

[47] D. Bento, A. I. Pereira, J. Lima, J. M. Miranda, and R. Lima, "Cell-free layer measurements of in vitro blood flow in a microfluidic network: an automatic and manual approach," *Comput. Methods Biomech. Biomed. Eng. Imaging Vis.*, vol. 6, no. 6, 2018.

[48] A. Kloosterman, C. Poelma, and J. Westerweel, "Flow rate estimation in large depth-of-field micro-PIV," *Exp. Fluids*, 2011.

[49] B. Chayer, K. L Pitts, G. Cloutier, and M. Fenech, "Velocity measurement accuracy in optical microhemodynamics: Experiment and simulation," *Physiol. Meas.*, 2012.

[50] C. D. Meinhart, S. Wereley, and M. Gray, "Volume illumination for two-dimensional particle image velocimetry," *Meas. Sci. Technol.*, 2000.

[51] K. L. Pitts and M. Fenech, "High speed versus pulsed images for micro-particle image velocimetry: A direct comparison of red blood cells versus fluorescing tracers as tracking particles," *Physiol. Meas.*, 2013.

[52] R. Rigler and E. Elson, "Fluorescence Correlation Spectroscopy Theory and Applications: Preface," *Springer Series in Chemical Physics*. 2001.

[53] K. Bacia, S. A. Kim, and P. Schwille, "Fluorescence cross-correlation spectroscopy in living cells," *Nat. Methods*, 2006.

[54] M. Brinkmeier, K. Dörre, J. Stephan, and M. Eigen, "Two-beam cross-correlation: A method to characterize transport phenomena in micrometer-sized structures," *Anal. Chem.*, 1999.

[55] D. Magde, W. W. Webb, and E. L. Elson, “Fluorescence correlation spectroscopy. III. Uniform translation and laminar flow,” *Biopolymers*, 1978.

[56] S. Wennmalm, P. Thyberg, L. Xu, and J. Widengren, “Inverse-fluorescence correlation spectroscopy,” *Anal. Chem.*, 2009.

[57] S. Wennmalm and J. Widengren, “Inverse-fluorescence cross-correlation spectroscopy,” *Anal. Chem.*, 2010.

[58] C. J. K. Armstrong, “Red Blood Cell Aggregation Characterization Using Norland Optical Adhesive Microfluidic Chips for a Reduction in Compliance,” 2020. [Online]. Available: https://ruor.uottawa.ca/handle/10393/40757. [Accessed: 24-Sep-2020].

[59] D. E. Bruns and W. C. Knowler, “Stabilization of glucose in blood samples: Why it matters,” *Clinical Chemistry*. 2009.

[60] R. Van Wijk and W. W. Van Solinge, “The energy-less red blood cell is lost: Erythrocyte enzyme abnormalities of glycolysis,” *Blood*, vol. 106, no. 13. American Society of Hematology, pp. 4034–4042, 15-Dec-2005.

[61] R. Mehri, “Red Blood Cell Aggregation Characterization: Quantification and Modeling Implications of Red Blood Cell Aggregation at Low Shear Rates,” 2016. [Online]. Available: https://ruor.uottawa.ca/handle/10393/35093. [Accessed: 24-Sep-2020].

[62] M. Fenech and L. Haya, “Blood Flow Mechanics,” in *Cardiovascular Mechanics*, Boca Raton, FL : CRC Press/Taylor & Francis Group, [2018]: CRC Press, 2018, pp. 63–89.